学位論文

Chiral symmetry and vacuum structure in rotating relativistic systems
(回転する相対論的システムにおける
カイラル対称性と真空構造)

平成 28 年 12 月博士（理学）申請

東京大学大学院理学系研究科
物理学専攻
豆田 和也

Chiral symmetry and vacuum structure

in rotating relativistic systems

Kazuya Mameda

Department of Physics, The University of Tokyo

December 2016

PhD Thesis

Abstract

Rotation is an intriguing subject not only from the academic viewpoint but also in the practical investigation of quantum matter. For Quantum Chromodynamics (QCD), the rotational effect is much crucial because rapid rotation actually exists in quark-hadron systems: rotating hot matter created in non-central relativistic heavy-ion collisions and rotating neutron stars. In this thesis, we analyze the QCD thermodynamics in rotating systems. First, we briefly review the relativistic scalar theory in a rotating frame. Then we find that for rotating systems the boundary condition plays a quite important role to correctly define the low-energy structure. Next we argue the thermodynamics of rotating fermionic matter. We prove that the rotational effect is invisible in the vacuum as long as the boundary condition is properly taken into account. In other words, rotation affects macroscopic quantities only if there is other external source, e.g. temperature, magnetic field. We show that in such environments, the rotational effect on the chiral symmetry breaking is quite similar to the finite-density effect. Especially for a magnetized rotating system, we discover that the interplay between magnetic field and rotation leads to the "rotational magnetic inhibition"; chiral symmetry for rotating fermions is restored by magnetic field. This is a novel phenomenon analogous to the inverse magnetic catalysis in a finite-density magnetized system. Finally, we qualitatively discuss that this phenomenon plays a crucial role to determine the chiral structure in the realistic systems.

Table of Contents

Chapter 1

Introduction

1.1   Chiral symmetry breaking in QCD

Quantum Chromodynamics (QCD) is the fundamental theory to describe the physics of the strong interaction. In principle thus, all of the dynamics of quarks and gluons is determined only from the QCD Lagrangian

$$\mathcal{L} = -\frac{1}{2}\operatorname{tr}[F_{\mu\nu}F^{\mu\nu}] + \bar{\psi}(i\gamma^{\mu}D_{\mu} - m)\psi\,, \tag{1.1}$$

where $F_{\mu\nu} = \partial_{\mu}A_{\nu} - \partial_{\nu}A_{\mu} + ig[A_{\mu}, A_{\nu}]$ is the field strength of gluon, ψ is the quark field, and $D_{\mu} = \partial_{\mu} + igA_{\mu}$ is the covariant derivative. One of the important features of QCD is the asymptotic freedom [1, 2]; the QCD running coupling constant $\alpha_s(Q)$ is weaken as the energy scale Q increases. At the one-loop level in the perturbation theory, the running coupling is calculated as $\alpha_s(Q) \sim \left[\ln(Q^2/\Lambda_{\mathrm{QCD}}^2)\right]^{-1}$, where $\Lambda_{\mathrm{QCD}} \simeq 200\,\mathrm{MeV}$ is the QCD energy scale. Because of this property, the perturbative QCD works very well for the physics in high-energy nuclear collision experiments [3]. On the other hand at low energy or short distance, the dynamics of quark and gluons is dominated by the nonperturbative effects, which lead to the quite complicated vacuum structure of QCD. For example, quarks and gluons are confined inside hadrons at low energy scale, unlike the ones in the high energy limit. This is so-called quark confinement. To investigate such an infrared phenomenon in QCD, we should employ nonperturbative frameworks.

The dynamical breaking of chiral symmetry is also one of the representative properties underlying in the nonperturbative vacuum structure of QCD. For the massless QCD with N_{f} flavors, the Lagrangian (1.1) is invariant under the transformation $\psi \to e^{i\theta_{\mathrm{V}}}\psi$ or $\psi \to e^{i\gamma_5\theta_{\mathrm{A}}}\psi$. That is, chiral symmetry $SU_{\mathrm{L}}(N_{\mathrm{f}}) \times SU_{\mathrm{R}}(N_{\mathrm{f}})$ holds. However this symmetry is dynamically broken through the strong interactions; $SU_{\mathrm{L}}(N_{\mathrm{f}}) \times SU_{\mathrm{R}}(N_{\mathrm{f}}) \to SU_{\mathrm{L+R}}(N_{\mathrm{f}})$. The spontanous breaking of chiral symmetry is manifested by the existence of (approximately) massless scalars, i.e. the Nambu–Goldstone bosons [4–6]. As a result of this, quarks acquire an additional mass of order of $\sim \Lambda_{\mathrm{QCD}}$. Since the chiral symmetry breaking is a nonperturbative phenomenon, it is much challenging problem to explain the dynamical mechanism from Eq. (1.1) (although the

chiral symmetry breaking itself is confirmed with the lattice QCD simulation). It was suggested by Nambu and Jona-Lasinio, however, that such a low-energy dynamics can be understood in the analogous manner to superconductivity [7, 8]; the dynamical mass is generated because of the condensate formed by a quark-antiquark pair (i.e. chiral condensate), similarly to the metallic superconducting energy gap coming from the condensate of the Cooper pair [9].

The analogy between the QCD vacuum and superconductor indicates that the phase transition in terms of the chiral symmetry is induced by external parameters (e.g. temperature), as well as the superconducting phase transition. In fact, chiral symmetry is restored at $T \gtrsim \Lambda_{\mathrm{QCD}} \simeq 10^{12}\,\mathrm{K}$, which corresponds to the temperature in early universe. The thermodynamic properties of the chiral symmetry breaking have been actively investigated by many nonperturbative analyses: the effective model studies [10–12], the remomalization group method for the Ginzburg–Landau function [13, 14]. Besides a lattice QCD simulation at finite temperature declares that the chiral phase transition is crossover in the practical case [15] (see also Ref. [16] as a review). On the other hand, the study for the chiral structure in finite-density systems is also be important for compact stars, which mostly consist of quarks and hadrons. An effective model analysis shows that the crossover chiral phase transition could be changed into the first-order one at finite density [17] (see also Ref [18]). Unfortunately, no firm verification for this suggestion has been given because lattice QCD does not work at finite chemical potential, which is known as the sign problem for the Monte-Calro simulation. To confirm the existence of this critical point at finite density (so-called the QCD critical point), we have to rely on heavy-ion collision experiments. Thus the thermodynamics of the QCD chiral structure is a much attractive subject not only theoretically but also experimentally [19, 20].

As well as temperature and chemical potential, several environmental sources modify the chiral structure in realistic systems. For example, external magnetic backgrounds exist in relativistic systems governed by the dynamics of chiral fermions; the early universe [21–23], in central cores of neutron stars (or magnetars) with $eB \simeq 10^{15}\,\mathrm{G}$ [24], and heavy-ion collisions with $eB \sim m_\pi^2 \simeq 10^{18}\,\mathrm{G}$ [25–27]. The crucial role of external magnetic field is the magnetic catalysis for the chiral symmetry breaking. Namely the chiral condensate in magnetic field is enhanced, and fermions always acquire the dynamical mass. The magnetic catalysis is confirmed from various theoretical approaches: the NJL model [28–31], the quark-meson model [32], the MIT bag model [33], the lattice QCD simulation [34], the holographic model [35] (see also Refs. [36, 37] and references therein). This phenomenon is also applicable to condensed matter with quasi-relativistic dispersions, i.e. the graphene [38, 39] and the Weyl semimetals [40].

More interestingly, the magnetic response of the chiral symmetry is drastically changed in a finite-density system. Contrary to magnetic backgrounds, density conduces to the restoration of chiral symmetry. Thus it naïvely seems that the chiral condensate in a magnetized finite-density system is simply determined through the competition between the enhancement by magnetic field and the suppression by chemical potential. However the interplay between these two effects realizes a more fruitful chiral structure. That is, at a finite chemical potential,

the chiral condensate is abolished by magnetic field. This curious magnetic response, which is so-called the inverse magnetic catalysis, is originally suggested from the analysis of a chiral model [31], and also this is rediscovered with a holographic QCD analysis [41, 42].

1.2 Rotational effects on quantum theory

As a external source, rotation leads to interesting physics in many quantum systems. An intriguing feature of rotation is to play a role of magnetic background. By rotating an atomic gas in a harmonic trap very rapidly, we can experimentally realize this correspondence [43–45]. Thus the Landau quantization and other magnetic phenomena are expected to be observable in rotating media: The quantum Hall effect is also induced by rotation instead of an external magnetic field [46]. A quantum vortex is generated by applying a magnetic field to the Bose-Einstein condensate or by rotating it [47, 48]. Besides the correspondence between magnetism and rotation is applied to non-central heavy-ion collisions; the experimental generation of rotating quark-gluon plasma is indicated by a global spin polarization [49–54]. In the leading order contribution of the derivative expansion of hydrodynamics, the vorticity appears as a fictitious magnetic field. Hence the chiral magnetic effect [55,56] and the chiral vortical effect [57,58] are categorized as similar transport phenomena in quark-gluon plasma (see Ref. [59] for a recent review for the anomalous transport phenomena). We note that the magnetic aspect underlying in rotation is not steady without an external source or an approximation. Indeed contrary to these cases, the relation between magnetism and rotation becomes unclear in relativistic field theory [60].

It is also important that rotation resembles density, and that this analogy is more ubiquitous than the one between rotation and magnetic field. In nonrelativistic theory, such an analogy is much clear in the sense that the Hamiltonian in rotating systems $H - \boldsymbol{\Omega} \cdot \boldsymbol{L}$ may be regarded as that with an effective chemical potential $\mu_{\text{eff}} = \boldsymbol{\Omega} \cdot \boldsymbol{L}$. It might seem that the similarity between rotation and density should hold for relativistic theories. However, this is not so trivial because according to general relativity, an influence of acceleration is regarded as a deformation of spacetime geometry. Thus the rotating quark-hadrons systems (heavy-ion collision, compact star, etc.) should be investigated based on the quantum field theory in curved spacetime [61], which is also utilized for the gravitational influence of the QCD vacuum structure [62–72] (see also Refs. [73–75] for quantum lattice simulations). If the analogy between rotation and density is found even in relativistic field theory, the QCD vacuum (especially the chiral structure) should be modified by rotation, as well as the density effect. From this motivation, in Ref. [76] (one of the main parts in this thesis), the author and collaborators have first manifested the rotational effect on chiral symmetry. Subsequently to this work, the rotational effect on the QCD matter has received more considerable attention [77–80]. In this thesis, we treat rotation as a thermodynamic source, and discuss the chiral symmetry breaking in rotating systems. Furthermore motivated by the finite-density inverse magnetic catalysis, we analyze the chiral

symmetry breaking in the presence of both magnetic field and rotation.

1.3   Boundary in rotating systems

In rotating systems, arbitrary spacetime point should rotate with keeping the causality con-
straint. This means that the thermodynamic limit (i.e. taking the infinitely large system size) is
not permitted for rotating systems; otherwise the velocity on the edge would exceed the speed
of light. Thus we should properly take into account the boundary effect, which is inevitable
under the presence of rotation.

Here let us intuitively see how the boundary effect is related to the rotational effect on
fermionic systems. For simplicity we consider the zero temperature case of the rotating cylinder
with radius R and angular velocity $\boldsymbol{\Omega} = \Omega \hat{z}$. For a fermion with j (the z-component of the
total angular momentum), the effective chemical potential reads Ωj. Thus a mode with the
energy lower than Ωj cannot be excited, and so it naïvely seems that the condensation of
fermionic paired states disappears at much large Ω. However this is the case without considering
the boundary effect. The transverse momentum is discretized in finite-size systems, and the
infrared mode has a finite energy gap as $\sim 1/R$. Furthermore such a gap depends on j, which
is understood as follows. A particle with large j possesses a wide orbital motion, which yields
a strong centrifugal force. Hence a larger energy cost is required to confine the particle in the
cylinder, and so each energy level (even the infrared gap) is pushed up as j grows. As a result,
we need to consider the competition between these two contributions: the effective chemical
potential and the infrared energy gap. In this thesis, we prove that this infrared energy gap
always defeats the effective chemical potential. This means that the rotational effect is invisible
unless temperature exceeds the effective chemical potential.

We note that the rotational effect is visible in some environments. One of the examples
is finite temperature because the thermal screening for $T \gg 1/R$ enables us to neglect the
boundary effect. In this thesis from a numerical calculation, we confirm that the dynamical
mass are affected by rotation at finite temperature. This is consistent with the fact that a
fermionic thermal radiation is induced by rotation at high temperature [81–83]. The second
example is the magnetic background. Once a magnetic field is applied, the wave function
of charged particles is localized with the width $\sim \ell_B \equiv 1/\sqrt{eB}$. At strong magnetic field
as $\ell_B \ll R$, it is expected that the particles do not receive the existence of the boundary.
Therefore even at zero temperature, the rotational effect is realized by a strong magnetic field.
In this thesis, we investigate the chiral structure in a magnetized rotating system. Also from
the viewpoint of the analogy between density and rotation, we expect that rotation could lead
to an inverse phenomenon of the magnetic catalysis. We name this novel phenomenon the
"rotational magnetic inhibition".

We emphasize that the proper treatment of the boundary condition is quite important
for the analysis of rotating systems, which has first been pointed out by the auther and the

collaborators [80]. If we took infinitely large radius, then the effective chemical potential could be larger than the energy gap. Indeed due to taking the thermodynamic limit for a rotating system, the authors in Ref. [77] have arrived at the incorrect result that angular velocity leads to phase transitions even at zero temperature.

1.4 Outline of this thesis

Chapter 2

We review the rotational effect in quantum theory, utilizing the case of rotating scalar particles. First we see how the rotational effect appears in nonrelativistic theory. Also based on quantum field theory in curved spacetime, we discuss the rotational effect in the relativistic case. Here we find that the boundary effect is important to determine the energy spectrum of rotating particles.

Chapter 3

We study the Dirac equation in the rotating cylinder, and discuss the discretization of the radial momentum for rotating fermions. With the solutions, we construct the Dirac propagator to analyze the dynamical breaking of chiral symmetry in rotating systems. We explicitly show that rotation never changes the thermodynamic quantities at zero temperature. Moreover within the NJL model, we compute the dynamical mass in a finite-size cylinder at zero temperature. We also calculate the dynamical mass in a rotating cylinder at finite temperature. We find that high temperature enables rotation to lead to the chiral restoration.

Chapter 4

We investigate the Dirac equation with both rotation and magnetic field. We find that the solution of the Dirac equation indicates that the modified Landau levels with rotation have nondegenerate spectrum with angular momentum dependence. Based on the resulting energy dispersion relation, we analyze the NJL model coupled with both magnetic field and rotation at zero temperature. Then we find that the chiral restoration is driven by increasing magnetic field. In other word, we obtain the inverse phenomenon of the magnetic catalysis induced by rotation, which we shall name "rotational magnetic inhibition". Also we discuss possible physical implications of our results.

Chapter 5

We summarize this thesis and mention the outlooks.

Appendix A

We solve the Dirac equation for rotating fermions without magnetic field, Eq. (3.6), and obtain the eigenfunction to construct the Dirac propagator. Also we solve the Dirac equation for rotating fermions with magnetic field, Eq. (4.9), and discuss only the energy spectrum, which enable us to analyze the dynamical symmetry breaking in Chapter 4 even without the eigenfunctions.

Appendix B

We discuss the Landau degeneracy factor in the cylindrical coordinate. From this, we identify the momentum phase space for rotating magnetized fermionic systems, Eq. (4.15).

Appendix C

We briefly review the NJL model, which we employ in Chapters 3 and 4.

Chapter 2

Basics of rotating systems

The dynamics of quantum systems is modified by rotation, as well as the classical mechanics. For the main purpose of this thesis, in this chapter, we briefly argue how the rotational effect should be treated quantum-mechanically. We review the nonrelativistic case, and based on this we consider the relativistic rotating scalar.

2.1 Nonrelativistic theory

First to catch a brief picture of the rotational effect on quantum particles, we see the nonrelativistic theory in a rotating system [47]. Let us consider the classical viscous fluid in a container, and define the nonrotating Hamiltonian as $H(\boldsymbol{x}, \boldsymbol{p})$ (for instance, $H(\boldsymbol{p}) = \boldsymbol{p}^2/(2m)$ in the case without the interaction between particles). Once the container rotates with angular velocity $\boldsymbol{\Omega}$, this fluid also rotates with the same $\boldsymbol{\Omega}$ due to the rotating wall of the container. This means that the dynamics is described by $H_{\mathrm{rot}}(\boldsymbol{x}, \boldsymbol{p})$, which includes all the influence of rotation. Since the rotating wall is a time-dependent external potential for the fluid, the problem is easily solved not in the rest frame $(\boldsymbol{x}, \boldsymbol{p})$ but in the frame co-rotating with the wall, $(\boldsymbol{x}', \boldsymbol{p}')$. Under the presence of rotation, the energy observed in the rest frame is the sum of the energy observed in the rotating frame and the rotational energy shift. Namely the Hamiltonian $H_{\mathrm{rot}}(\boldsymbol{x}', \boldsymbol{p}')$ is given by [84]

$$H_{\mathrm{rot}}(\boldsymbol{x}', \boldsymbol{p}') = H(\boldsymbol{x}', \boldsymbol{p}') - \boldsymbol{\Omega} \cdot \boldsymbol{L}(\boldsymbol{x}', \boldsymbol{p}'), \tag{2.1}$$

where $\boldsymbol{L} = \boldsymbol{x}' \times \boldsymbol{p}'$ is angular momentum in the rotating frame. For the observer in the rotating frame, the rotational effect appears only in the rotational energy shift. We emphasize that this comes from the coordinate transformation to the external potential of the wall seems stationary. From this Hamiltonian, we find the following important properties of rotation.

(I) Inhomogeneity induced by rotation

In the case without the interaction term, the Hamiltonian in the rotating frame with $\boldsymbol{\Omega} = \Omega\hat{z}$

can be written as

$$H_{\text{rot}} = \frac{1}{2m}(\boldsymbol{p} - m\Omega\hat{z} \times \boldsymbol{x})^2 - \frac{1}{2}m\Omega^2(x^2 + y^2) \,, \tag{2.2}$$

where coordinate $\boldsymbol{x}$ and momentum $\boldsymbol{p}$ are redefined as the valuables in the rotating frame (hereafter we drop the prime symbol). The second term corresponds to the potential leading to the centrifugal force:

$$\boldsymbol{\nabla}\left[\frac{1}{2}m\Omega^2(x^2 + y^2)\right] = m\boldsymbol{\Omega} \times \left(\boldsymbol{\Omega} \times \boldsymbol{x}\right). \tag{2.3}$$

Namely in rotating systems, the potential in Eq. (2.2) realizes an inhomogeneity along the direction perpendicular to the rotating axis. Because of such an inhomogeneity, the local free energy is dependent on the radial coordinate $r = \sqrt{x^2 + y^2}$. Besides for a theory involving a spontaneous symmetry breaking, the energy gap becomes a function of r. In this thesis, within the Nambu–Jona-Lasinio model in rotating frames, we discuss the inhomogeneity of the dynamical mass.

On the other hand, the first term in Eq. (2.2) is not irrelevant to the inhomogeneity. To understand this, we consider the charged nonrelativistic particle in a constant magnetic field $\boldsymbol{B} = B\hat{z}$. If we adopt the gauge $\boldsymbol{A} = B\hat{z} \times \boldsymbol{x}/2$, the corresponding Hamiltonian reads

$$H_{\text{mag}} = \frac{1}{2m}(\boldsymbol{p} - eB\hat{z} \times \boldsymbol{x}/2)^2 \,, \tag{2.4}$$

which is equivalent to the first term in Eq. (2.2) under the replacement

$$eB \leftrightarrow 2m\Omega \,. \tag{2.5}$$

This gives the classical correspondence between the Coriolis force $\boldsymbol{F}_{\text{Coriolis}} = 2m\dot{\boldsymbol{x}} \times \boldsymbol{\Omega}$ and the Lorentz force $\boldsymbol{F}_{\text{Lorentz}} = e\dot{\boldsymbol{x}} \times \boldsymbol{B}$. The magnetized Hamiltonian (2.4) seems to break the translational invariance on the xy-plane. However, magnetic field $\boldsymbol{B} = B\hat{z}$ does not lead to the inhomogeneity as long as the system size is much larger than the magnetic length scale $\ell_B \equiv 1/\sqrt{eB}$. Therefore, the kinetic term of rotating particles does not generate to an inhomogeneity if angular velocity keeps the following condition:

$$1/\sqrt{m\Omega} \ll R \,, \tag{2.6}$$

where R is the system size scale on the xy-plane. Indeed the above inequality is always satisfied in the nonrelativistic limit; $m\Omega = mc^2 \times \Omega/c = m\Omega c \to \infty$, where c is the speed of light.

Furthermore the correspondence (2.5) implies that rotation could lead to magnetic phenomena. In fact, rotation plays the role of magnetic field if the centrifugal force potential is experimentally cancelled out by applying the external trapping potential

$$V_{\text{trap}} = \frac{1}{2}m\Omega^2(x^2 + y^2) \,. \tag{2.7}$$

As a result the spectra for the motion on the xy-plane become the Landau levels. In this way, a rotating Bose-Einstein condensate realizes the quantum Hall effect [46] or forms quantum vortex [47, 48]. Also in the study of heavy-ion collision, the rotational effect is regarded as a fictitious magnetic field. In the hydrodynamic description, a vorticity (i.e. the angular velocity for local rotation) is defined as the derivative of fluid velocity. In the leading order level of the derivative expansion, the higher order terms of the vorticity, such as the second term in Eq. (2.4), do not appear. Thus magnetic field and vortex lead to similar anomalous transport phenomena in quark-gluon plasma; $\boldsymbol{j} \propto \boldsymbol{B}$ and $\boldsymbol{j} \propto \boldsymbol{\Omega}$, which are so-called the chiral magnetic effect [55, 56] and the chiral vortical effect [57, 58], respectively.

(II) Analogy between rotation and density

From Eq. (2.1), we find that rotation resembles density rather than magnetic field. This analogy is easily understood by identifying the rotational energy shift as an effective chemical potential:

$$\mu_\ell \equiv \Omega\ell\,, \tag{2.8}$$

where ℓ represents the quantum number for L_z (the z-component of $\boldsymbol{L}$). Thus thermodynamic quantities of rotating particles would be calculated similarly to that in finite-density systems. For example, it is naïvely expected that the Bose-Einstein distribution function for the mode with angular momentum ℓ is given by

$$n_{\mathrm{BE}} = \frac{1}{e^{\beta(\varepsilon - \Omega\ell)} - 1}\,, \tag{2.9}$$

where ε is the energy observed in the rest frame. The physical meaning of Eq. (2.9) is explained as follows. Because of the centrifugal force, a particle tend to rotate at a large distance from the rotation axis, and thus it possesses large angular momentum. As a result, for given ε, the distribution of modes with large ℓ is greater.

We should mention the exponent in Eq. (2.9). In finite-density systems, chemical potential cannot be larger than the energy of particles so that the distribution function can be positive at arbitrary temperature. On the other hands, it seems that the effective chemical potential could exceed the particle energy as Ω increases. Such a pathological situation necessarily occurs because the nonrelativistic discussion is available only for small $\Omega = \Omega/c$. Therefore for large Ω, rotation should be treated based on general relativity. More precisely, we should employ the quantum theory in non-flat spacetime that is called quantum field theory in curved spacetime. Indeed in this framework, we derive that Eq. (2.9) is always positive, namely, $\varepsilon > \Omega\ell$ for arbitrary ℓ.

2.2   Relativistic theory

We here consider relativistic particles confined in the system that has rotating boundary. As we discussed in the previous section, the rotating frame is more appropriate in this case than the inertial frame. From the relativistic viewpoint, thus we need quantum field theory in curved spacetime. Compared with the flat (Minkowski) spacetime case, the major differences are the following three.

(I) Metric tensor

As the generalization of quantum field theory in flat spacetime, the contraction of indices in vectors and tensors is taken with the corresponding metric. Besides the effects of spacetime geometry are introduced not only by the metric but also vierbein. These two are related as

$$g^{\mu\nu} = \eta^{ij} e_i^\mu e_j^\nu \,, \tag{2.10}$$

where η^{ij} is the Minkowski metric. Here Greek (Latin) indices, $\mu = t, x, y, z$ ($i = 0, 1, 2, 3$), denote coordinate (tangent) space. We note that vierbein is not determined uniquely even if a metric is designated. Indeed the representation of rotating Dirac fermions depends on the choice of vierbein [85, 86].

(II) Covariant derivative

In gauge theory, the gauge-invariance of a derivative term is remained by introducing the covariant derivative, i.e. $\partial_\mu \to D_\mu$. Similarly to keep the invariance under the general coordinate transformation, a corresponding covariant derivative is necessary:

$$\partial_\mu \to \nabla_\mu \,. \tag{2.11}$$

The specific expression of ∇_μ is dependent on what the derivative acts on, such as scalar, spinor, and so on.

(III) Fock space

In general, the coordinate transformation changes not only operators but also the Fock space, and thus the expectation value of physical quantities is dependent on the coordinate of observer. Because of this, even if a field is observed as a particle (i.e. the positive-energy mode) in the Minkowski coordinate, it can be observed as an antiparticle (i.e. the negative-energy mode) in a different frame. This is mathematically described as the Bogoliubov transformation of the creation and annihilation operators. Once the Bogoliubov coefficient becomes nonzero, a particle production takes place. Indeed, such a phenomenon in a black hole and in a linearly accelerating frame are called the Hawking and Unruh radiation, respectively. It should be mentioned that both cases possesses a horizon (a fictitious horizon), and that the existence of

it plays the essential role to change the vacuum state. Therefore this is not the case for the transformation to rotating frames (at least as long as the causality constraint holds), as we discuss in a later part of the section.

Now let us see the free real scalar theory. The action is described by

$$S_\phi = \int d^4 x \sqrt{|\det g|} \left[g^{\mu\nu} \partial_\mu \phi \, \partial_\nu \phi + m^2 \phi^2 \right] , \qquad (2.12)$$

where the covariant derivative for scalar is given by $\nabla_\mu = \partial_\mu$. The generalized four dimensional volume factor $d^4 x \sqrt{|\det g|}$ is invariant under the general coordinate transformation. From the action (2.12), the classical equation of motion for $\phi(x)$ is obtained as

$$\left[\frac{1}{\sqrt{|\det g|}} \, \partial_\mu \sqrt{|\det g|} \, g^{\mu\nu} \partial_\nu + m^2 \right] \phi(x) = 0 . \qquad (2.13)$$

When we consider an infinitely long rotating cylinder with angular velocity $\boldsymbol{\Omega} = \Omega \hat{z}$ with $\Omega > 0$ (see Fig. 2.1), the corresponding metric tensor reads

$$g_{\mu\nu} = \begin{pmatrix} 1 - (x^2 + y^2)\Omega^2 & y\Omega & -x\Omega & 0 \\ y\Omega & -1 & 0 & 0 \\ -x\Omega & 0 & -1 & 0 \\ 0 & 0 & 0 & -1 \end{pmatrix} . \qquad (2.14)$$

Since we are interested in a physically possible rotating system, the relativistic causality in terms of rotation should be respected everywhere in the system. Thus it is necessary that the velocity on the edge of the cylinder cannot be grater than the speed of light:

$$v_{\text{edge}} = R\Omega \leq 1 , \qquad (2.15)$$

where the radius of the cylinder is defined as R (see Fig. 2.1).

In the rotating frame (2.14), the Klein–Gordon equation (2.13) is reduced to

$$\left[\left\{ \partial_0 + \Omega(x\partial_y - y\partial_x) \right\}^2 - \partial_1^2 - \partial_2^2 - \partial_3^2 + m^2 \right] \phi(x) = 0 . \qquad (2.16)$$

The product of the angular velocity and angular momentum corresponds to the rotational energy, and for $\Omega = 0$ this is the same as the equation in the Minkowski spacetime. The equation is a natural form because the energy of particles in a rotating frame is shifted by the rotational energy; $H \to H - \boldsymbol{\Omega} \cdot \boldsymbol{L}$.

If we adopt the cylindrical coordinate, the solution for Eq. (2.16) is easily found as

$$\phi = e^{-iEt + ip_z z + i\ell\theta} J_\ell(p_\perp r) \qquad (2.17)$$

with the Bessel function $J_\ell(p_\perp r)$. Also the energy spectrum is obtained as

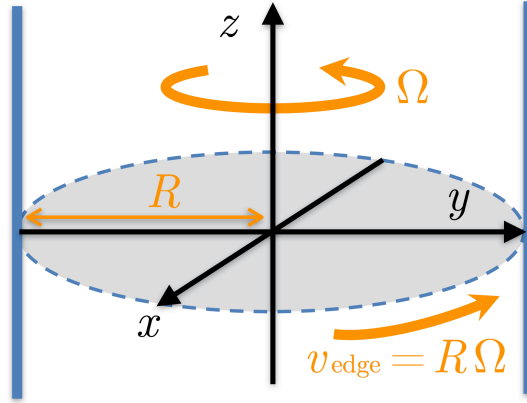$$E = \pm\varepsilon - \Omega\ell , \qquad (2.18)$$

Figure 2.1: Rotating cylindrical system. Because of the relativistic causality, the velocity on the edge of the cylinder cannot exceed the speed of light; $v_\text{edge} = R\Omega \leq 1$

where the radial momentum $p_\perp$ is defined by $\varepsilon = \sqrt{p_\perp^2 + p_z^2 + m^2}$. We note that ε is the energy of rotating particles observed in the Minkowski coordinate, and thus E corresponds to the energy seen by the co-rotating observer.

Since the angular momentum ℓ can be arbitrary integer, the spectrum (2.18) seems unbounded. This problem comes from the invalid assumption that the system size is infinitely large. If we consider the rotating system that dose not violate the causality constraint, the radius of the rotating cylinder R cannot be infinite because of $R \leq 1/\Omega < \infty$. As a result, the radial momentum $p_\perp$ should be discretized unlike p_z (we here suppose an infinitely long cylinder along the z-direction).

Here let us impose the Dirichlet boundary condition, i.e. $J(p_\perp R) = 0$. Then the discrete momentum is obtained as

$$p_\perp \equiv p_{\ell,k} = \xi_{\ell,k}/R \,, \tag{2.19}$$

where $\xi_{\ell,k}$ represents the kth zero of $J_\ell(z)$. This discretized momentum ensures that the spectrum (2.18) is definitely bounded, as follows. First the lower bound of $E = \varepsilon - \Omega\ell$ is determined as

$$E \geq \frac{\xi_{\ell,1}}{R} - \Omega\ell = \frac{1}{R}(\xi_{\ell,1} - R\Omega\ell) \,. \tag{2.20}$$

Also the lowest zeros satisfy $\xi_{\ell,1} > |\ell|$, which follows from the following inequalities [87]:

$$\begin{aligned} \xi_{\ell,1} &= 2.40483 \quad \text{for} \quad \ell = 0 \,, \\ \xi_{\ell,1} &> \ell + 1.855757\ell^{1/3} + 0.5\ell^{-1/3} \quad \text{for} \quad \ell \geq 1 \,. \end{aligned} \tag{2.21}$$

Therefore $E = \varepsilon - \Omega\ell$ is lower-bounded as long as causality is kept (i.e. $R\Omega \leq 1$). Similarly, it is proved that the negative-sign spectrum is upper-bounded; $E = -\varepsilon - \Omega\ell < 0$. In Fig. 2.2, we plot the lowest positive-sign spectrum for $p_z = m = 0$, i.e. $E = \xi_{\ell,1}/R - \Omega\ell$. This plot shows that the ground state is always $\ell = 0$ even for $\Omega > 0$.
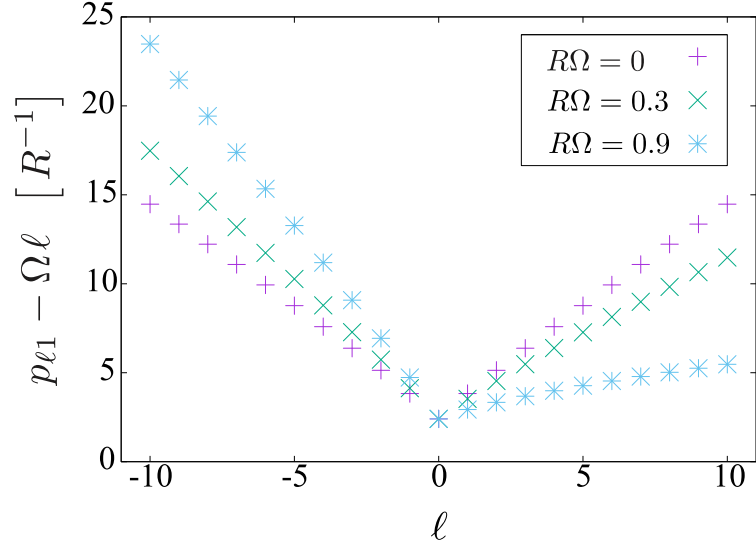
Figure 2.2: Positive-sign spectrum in Eq. (2.18) with $p_z = m = 0$ and $p_{\ell,k} = p_{\ell,1} = \xi_{\ell,1}/R$ [60]. The $\ell = 0$ mode always corresponds to the ground state. In rotating frames ($\Omega \neq 0$), the positive ℓ modes are more energetically-favorable than the ℓ modes.

We should here mention the Fock space in the rotating coordinate. As discussed above, the sign of E coincidences with that of ε, and thus the positive- and negative-energy are never mixed even under the transformation between the Minkowski and rotating coordinate. Hence the rotating vacuum is equivalent to the Minkowski one, and the creation and annihilation operators are also the same in both frames; $|0_M\rangle = |0_R\rangle \equiv |0\rangle$, and $a_M^\dagger = a_R^\dagger \equiv a^\dagger$. Because of this, the zero temperature field theory is unchanged regardless whether rotation is applied or not. In other words, rotation cannot be realized in the vacuum.

Contrary to the zero temperature case, rotation definitely affects the system at finite temperature. As discussed in Ref. [84], the rotational effect on thermodynamics is introduced through the density operator

$$\rho = e^{-\beta(H - \boldsymbol{\Omega} \cdot \boldsymbol{L})} \big/ \mathrm{tr}\left[e^{-\beta(H - \boldsymbol{\Omega} \cdot \boldsymbol{L})}\right], \tag{2.22}$$

where H is the Hamiltonian corresponding to the energy observed in the Minkowski frame. Hence the thermodynamics in rotating systems is constructed in the imaginary-time formalism, similarly to the one in the flat spacetime. For example the Bose-Einstein distribution function for a rotating particle is obtained as

$$\begin{aligned} n_{\mathrm{BE}}(\ell, k, p_z) &\equiv \langle a_{\ell,k,p_z}^\dagger a_{\ell,k,p_z} \rangle_\beta \\ &= \frac{1}{e^{\beta(\varepsilon - \Omega\ell)} - 1} \end{aligned} \tag{2.23}$$

with $\varepsilon = \sqrt{p_{\ell,k}^2 + p_z^2 + m^2}$. Here the thermal expectation value is defined as $\langle O \rangle_\beta \equiv \mathrm{tr}[\rho\, O]$. The inequality $\varepsilon > \Omega\ell$ for arbitrary ℓ ensures that the expectation value in the rotating Minkowski

frame is reproduced from Eq. (2.23) in the zero temperature limit:

$$\langle a^\dagger_{\ell,k,p_z} a_{\ell,k,p_z} \rangle_\beta \xrightarrow[\beta\to\infty]{} \langle 0 | a^\dagger_{\ell,k,p_z} a_{\ell,k,p_z} | 0 \rangle = 0 \ . \tag{2.24}$$

Therefore the distribution for rotating bosons is thermodynamically well-defined, as mentioned in the previous section.

We emphasize again that the boundary effect is most essential in the above argument. If we permitted an infinitely large R, the radial momentum $p_\perp$ would be continuous valuable independent of angular momentum ℓ. In this case, since $\varepsilon \le \Omega\ell$ could be allowed for a large ℓ, we would not arrive at Eq. (2.24). Similarly such an undesirable situation emerges for rotating fermions unless we properly treat the boundary effect. We also note that such a boundary condition is physically necessary because we assume that the rotation of relativistic particles is driven due to the rotating wall of the cylindrical system. The same is true for fermionic matter. Unfortunately the boundary condition for spinors in rotating systems is not so trivial as scalars. In the following chapter, we discuss the boundary condition for rotating fermions in a finite-size cylinder, and then obtain a discretized momentum similar to Eq. (2.19).

Chapter 3

Chiral symmetry with rotation

Chiral symmetry is one of the most important concepts to identify the state of the QCD matter. Its breaking structure is quite sensitive to environmental sources, such as temperature, density, and electromagnetic backgrounds. In this chapter, from the viewpoint of the analogy to the density effect, we discuss the rotational effect of the chiral symmetry breaking.

3.1 Dirac equation

The Dirac theory in the curved spacetime reads

$$S_\psi = \int d^4x \sqrt{|\det g|}\, \bar{\psi}\big[i\gamma^\mu(\partial_\mu + \Gamma_\mu) - m\big]\psi\,, \tag{3.1}$$

Gamma matrices in flat spacetime and the one in curved spacetime are related as $\gamma^\mu = \gamma^i e_i^\mu$. The covariant derivative $\nabla_\mu = \partial_\mu + \Gamma_\mu$ is defined with

$$\text{affine connetcion}: \Gamma_\mu = -\frac{i}{4}\omega_{\mu ij}\sigma^{ij}\,,$$
$$\text{spin connetcion}: \omega_{\mu ij} = g_{\alpha\beta}e_i^\alpha(\partial_\mu e_j^\beta + \Gamma_{\mu\nu}^\beta e_j^\nu)\,, \tag{3.2}$$
$$\text{spin matrix}: \sigma^{ij} = \frac{i}{2}[\gamma^i, \gamma^j]\,,$$

where $\Gamma_{\mu\nu}^\alpha$ denotes the Christoffel symbol. From the fermion action (3.1), the Dirac equation in a curved spacetime is given by

$$\big[i\gamma^\mu(\partial_\mu + \Gamma_\mu) - m\big]\psi = 0\,. \tag{3.3}$$

Now let us assume that fermions confined in a rotating cylindrical container with angular velocity $\boldsymbol{\Omega} = \Omega\hat{z}$ (see Fig. 2.1). Namely we assume that a rigid rotation is realized in a fermionic fluid system. Although realistic rotating QCD systems might not be so simple, such a ideal picture should be quite useful to pick up typical features of rotating fermions. For example, for the rotating matter generated in the ultrarelativistic heavy-ion collisions, the transverse size scale of it corresponds to the radius R in the cylinder (see Figure 3.1). Also the angular
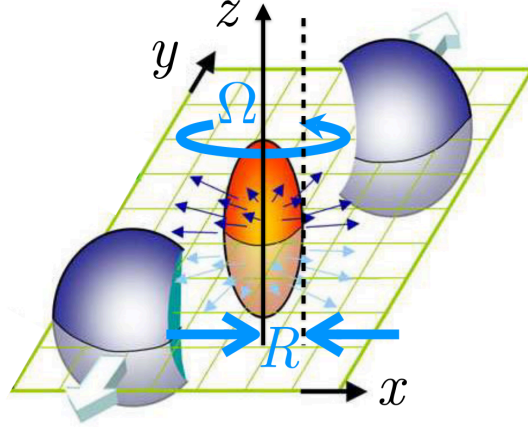
Figure 3.1: Schematic picture of the rotating matter produced in heavy-ion collision experiment. Noncentral heavy-ion collisions on the xy-plane produces the hot QCD matter with a finite angular momentum along the z-direction. The rotating cylinder depicted in Fig. 2.1 is the simplest version of this system.

velocity of the boundary of the rotating cylinder is replaced with the one driven externally by the colliding heavy-ions.

The corresponding metric is hence the same as Eq. (2.14):

$$
g_{\mu\nu} = \begin{pmatrix} 1 - (x^2 + y^2)\Omega^2 & y\Omega & -x\Omega & 0 \\ y\Omega & -1 & 0 & 0 \\ -x\Omega & 0 & -1 & 0 \\ 0 & 0 & 0 & -1 \end{pmatrix} . \tag{3.4}
$$

In this thesis we adopt the vierbein as

$$
e_0^t = e_1^x = e_2^y = e_3^z = 1, \qquad e_0^x = y\Omega, \qquad e_0^y = -x\Omega , \tag{3.5}
$$

and zero for other components. From the above metric and vierbein, we reduce the Dirac equation in the rotating frame to the following form:

$$
\left[i\gamma^0 \left\{ \partial_0 + \Omega \left(x\partial_2 - y\partial_1 + \frac{i}{2}\sigma^{12} \right) \right\} + i\gamma^1\partial_1 + i\gamma^2\partial_2 + i\gamma^3\partial_3 - m \right] \psi = 0 . \tag{3.6}
$$

As well as in scalar theory, rotation here appears only through the rotational energy shift, $H \to H - \Omega(L_z + S_z)$. Namely the Dirac fermions in rotating frames behave as if they were put at the finite-density systems with a chemical potential

$$
\mu = \Omega(\ell + s_z) , \tag{3.7}
$$

where the quantum number ℓ and s_z denote the eigenvalue for L_z and S_z, respectively. We should note that due to this similarity, the fermions under rotation also involve the sign problem for Monte Carlo simulations [73].

In the Dirac representation, the positive-energy solution with positive and negative helicity for the Dirac equation (3.6) are obtained as follows:

$$u_+ = \frac{e^{-iEt+ip_z z}}{\sqrt{\varepsilon + m}} \begin{pmatrix} (\varepsilon + m)\phi_{\ell,k} \\ 0 \\ p_z\,\phi_{\ell,k} \\ ip_{\ell,k}\,\varphi_{\ell,k} \end{pmatrix}, \quad u_- = \frac{e^{-iEt+ip_z z}}{\sqrt{\varepsilon + m}} \begin{pmatrix} 0 \\ (\varepsilon + m)\varphi_{\ell,k} \\ -ip_{\ell,k}\,\phi_{\ell,k} \\ -p_z\,\varphi_{\ell,k} \end{pmatrix}, \tag{3.8}$$

where $\varepsilon \equiv |E + \Omega(\ell + 1/2)|$ is the energy observed in the Minkowski frame, and the transverse momentum is defined with $p_{\ell,k}^2 = \varepsilon^2 - p_z^2 - m^2$. The quantum number k is determined from the boundary condition that we discuss later, and so this k is slightly different from that for rotating scalars, i.e. Eq. (2.19). The solution in the above expressions is not normalized, but the normalization factors are properly given once the momentum phase space with respect to ℓ and k is identified. In the above solutions we introduce the scalar functions

$$\phi_{\ell,k} \equiv e^{i\ell\theta} J_\ell(p_{\ell,k} r), \quad \varphi_{\ell,k} \equiv e^{i(\ell+1)\theta} J_{\ell+1}(p_{\ell,k} r), \tag{3.9}$$

where $J_\ell(x)$ is the ℓth Bessel function of the first kind. From the charge conjugation $v_\pm = i\gamma^2 u_\pm^*$, the negative-energy antiparticle solutions are also obtained as

$$v_+ = \frac{e^{iEt-ip_z z}}{\sqrt{\varepsilon + m}} \begin{pmatrix} -ip_{\ell,k}\,\varphi_{\ell,k}^* \\ -p_z\,\phi_{\ell,k}^* \\ 0 \\ (\varepsilon + m)\phi_{\ell,k}^* \end{pmatrix}, \quad v_- = \frac{e^{iEt-ip_z z}}{\sqrt{\varepsilon + m}} \begin{pmatrix} -p_z\,\varphi_{\ell,k}^* \\ -ip_{\ell,k}\,\phi_{\ell,k}^* \\ -(\varepsilon + m)\varphi_{\ell,k}^* \\ 0 \end{pmatrix}. \tag{3.10}$$

The detail of the calculation is shown in Appendix A.1.

Here we should mention the spin of $u_\pm$. Since the z-component of the total angular momentum is a good quantum number, $u_\pm$ is an eigenfunction for it. Indeed the azimuthal angular momentum of spin-up and -down are related to each other as $\ell = \ell_+ = \ell_- - 1$ so that both of the up and down spin states has the same total angular momentum; $\ell_+ + 1/2 = \ell_- - 1/2 \equiv j$. For the same reason, the solution $u_\pm$ consists of $\phi_{\ell,k}$ and $\varphi_{\ell,k}$, which correspond to the ℓ_+ and ℓ_- state, respectively.

3.2 Momentum discretization

In rotating systems, the boundary effect should be properly taken into account because of $R \leq 1/\Omega < \infty$. In the scalar case, the momentum discretization is easily obtained with the Dirichlet boundary condition. Unfortunately such a trivial condition is not applicable to rotating fermions [83]. Instead it is necessary to find a different boundary condition for rotating fermions.

Here we adopt the boundary condition about the fermionic current. If the vector current $j^\mu = \bar{\psi}\gamma^\mu\psi$ is conserved in a curved spacetime, the following equation holds:

$$\frac{1}{\sqrt{|\det g|}}\partial_\mu(\sqrt{|\det g|}\,j^\mu) = 0\,. \tag{3.11}$$

This is equivalent to the boundary condition that there is no incoming flux of the fermions:

$$\int_V dV\,\partial_\alpha(\sqrt{|\det g|}\,\bar{\psi}\gamma^\alpha\psi) = \int_{\partial V} d\Sigma_\alpha\sqrt{|\det g|}\,\bar{\psi}\gamma^\alpha\psi = 0\,, \tag{3.12}$$

where α stands for the spatial components x, y, z in coordinate space. In the rotating coordinate defined by Eq. (3.4), the above equation is reduced to

$$R\int_{-\infty}^\infty dz\int_0^{2\pi} d\theta\,\bar{\psi}\gamma^r\psi\Big|_{r=R} = 0\,. \tag{3.13}$$

Here we introduced $\gamma^r \equiv \gamma^1\cos\theta + \gamma^2\sin\theta$ that follows from $\gamma^1\partial_1 + \gamma^2\partial_2 = \gamma^r\partial_r + r^{-1}\gamma^\theta\partial_\theta$. Expanding $\psi(x)$ with the complete set of $u_\pm(x)$ and $v_\pm(x)$, Eq. (3.13) gives the boundary condition at $r = R$ for the arbitrary solution of Eq. (3.6). Namely after performing the θ-integral, Eq. (3.13) are represented only with the liner combination of the following products:

$$J_\ell(p_{\ell,k}R)J_{\ell+1}(p_{\ell,k'}R)\,,\quad J_{\ell+1}(p_{\ell,k}R)J_\ell(p_{\ell,k'}R)\,,$$
$$J_\ell(p_{\ell,k}R)J_{\ell+1}(p_{-\ell-1,k'}R)\,,\quad J_{\ell+1}(p_{\ell,k}R)J_\ell(p_{-\ell-1,k'}R)\,.$$

In order to realize the no-flux condition for the arbitrary solution of Eq. (3.6), it is necessary to vanish all of the four simultaneously. Therefore the radial momentum should be discretized as follows [88, 89]:

$$p_{\ell,k} = \begin{cases} \xi_{\ell,k}/R & \text{for}\quad \ell = 0, 1, \dots \\ \xi_{-\ell-1,k}/R & \text{for}\quad \ell = -1, -2, \dots \end{cases} \tag{3.14}$$
$$= \xi_{|j|-1/2,k}/R\,.$$

This expression is consistent with the fact that the total angular momentum $j = \ell + 1/2$ is a good quantum number.

Let us discuss the momentum phase space in the cylindrical systems. The modification of the phase space is obtained from the normalization for $u_\pm$ and $v_\pm$. Because of the discretization (3.14), the inner products of $\phi_{\ell,k}$ and $\varphi_{\ell,k}$ is calculated as

$$\int_0^R rdr\int_0^{2\pi} d\theta\,\phi_{\ell,k}^*\phi_{\ell'k'} = \int_0^R rdr\int_0^{2\pi} d\theta\,\varphi_{\ell,k}^*\varphi_{\ell'k'} = \pi R^2 J_{\ell+1}(p_{\ell,k}R)^2\delta_{\ell\ell'}\delta_{kk'}\,. \tag{3.15}$$

Here we used the following relation:

$$\int_0^R dr\,r\,J_\ell(p_{\ell,k}r)J_\ell(p_{\ell k'}r) = \int_0^R dr\,r\,J_{\ell+1}(p_{\ell,k}r)J_{\ell+1}(p_{\ell k'}r) = \frac{R^2}{2}\delta_{kk'}J_{\ell+1}(p_{\ell,k}R)^2\,. \tag{3.16}$$

Therefore in the cylindrical coordinate, the integration of the momentum phase space is changed as

$$\int \frac{dp_x dp_y}{(2\pi)^2} \, \mathcal{I}(p_x, p_y) \to \frac{1}{\pi R^2} \sum_{\ell=-\infty}^{\infty} \sum_{k=0}^{\infty} \frac{1}{J_{\ell+1}(p_{\ell,k}R)^2} \, \mathcal{I}(\ell, k) \ . \tag{3.17}$$

We note that for $\Omega = 0$ and $R \to \infty$, this modified phase space should become the one in the flat Minkowski spacetime. In other words, as R increases, the ℓ- and k-sum involving these factors is approximately reduced as the integral of the radial momentum:

$$\frac{1}{\pi R^2} \sum_{k} \frac{1}{J_{\ell+1}(p_{\ell,k}R)^2} \approx \frac{1}{2\pi} \sum_{k} p_{\ell,k} \, \Delta p_{\ell,k} \xrightarrow[R\to\infty]{} \int \frac{d\boldsymbol{p}_\perp}{(2\pi)^2} \ , \tag{3.18}$$

where $\Delta p_{\ell,k} \equiv p_{\ell,k+1} - p_{\ell,k}$. We have numerically confirmed that this approximation is applicable for not too large ℓ; for example, the deviation at $\ell = 100$ and $k = 10$ is around one percent, and the precision grows for smaller ℓ.

3.3   NJL model

To compute the chiral condensate in rotating frames, we first construct the Dirac propagator for rotating fermions. From $u_\pm(x)$ and $v_\pm(x)$, which build $\psi(x)$ and $\bar{\psi}(x)$, the following propagator is straightforwardly obtained:

$$S_F^{\alpha\beta}(x, x') = i \int \frac{dp^0 dp_z}{(2\pi)^2} \sum_{\ell=-\infty}^{\infty} \sum_{k=1}^{\infty} \frac{1}{\pi R^2 J_{\ell+1}(p_{\ell,k}R)^2}$$
$$\times \frac{e^{-ip^0(t-t')+ip_z(z-z')}}{(p^0 + \Omega j)^2 - \varepsilon^2 + i\epsilon} \mathcal{S}^{\alpha\beta}(p; r, \theta, r', \theta') \ . \tag{3.19}$$

Here we defined the spinor matrix as

$$\mathcal{S} = \begin{pmatrix} (p_0 + m)\phi_{\ell,k}\phi'_{\ell,k} & 0 & -p_z\phi_{\ell,k}\phi'_{\ell,k} & ip_{\ell,k}\phi_{\ell,k}\varphi'_{\ell,k} \\ 0 & (p_0 + m)\varphi_{\ell,k}\varphi'_{\ell,k} & -ip_{\ell,k}\varphi_{\ell,k}\phi'_{\ell,k} & p_z\varphi_{\ell,k}\varphi'_{\ell,k} \\ -p_z\phi_{\ell,k}\phi'_{\ell,k} & -ip_{\ell,k}\phi_{\ell,k}\varphi'_{\ell,k} & (-p_0 + m)\phi_{\ell,k}\phi'_{\ell,k} & 0 \\ ip_{\ell,k}\varphi_{\ell,k}\phi'_{\ell,k} & p_z\varphi_{\ell,k}\varphi'_{\ell,k} & 0 & (-p_0 + m)\varphi_{\ell,k}\varphi'_{\ell,k} \end{pmatrix} , \tag{3.20}$$

where we used simpler notations for the matrix elements; $\phi_{\ell,k}(r, \theta) \equiv \phi_{\ell,k}$, $\phi_{\ell,k}(r', \theta') \equiv \phi'_{\ell,k}$, and so on. For $\Omega = 0$ and $R \to \infty$, this propagator should be the one in the flat Minkowski

spacetime:

$$
\begin{aligned}
S_F(x, x')\big|_{\Omega=0, R\to\infty} & \\
= i \int \frac{d^4p}{(2\pi)^4} & \frac{e^{-ip^0(t-t')+ip_z(z-z')}}{(p^0)^2 - \varepsilon^2 + i\epsilon} \left[(\gamma^0 p^0 - \gamma^3 p_z + m) J_0(p_\perp |\boldsymbol{r} - \boldsymbol{r}'|) \right. \\
& \left. - i \left\{ (r\cos\theta - r'\cos\theta')\gamma^1 + (r\sin\theta - r'\sin\theta')\gamma^2 \right\} \frac{p_\perp J_1(p_\perp |\boldsymbol{r} - \boldsymbol{r}'|)}{|\boldsymbol{r} - \boldsymbol{r}'|} \right] \qquad (3.21) \\
= i \int \frac{d^4p}{(2\pi)^4} & \frac{\gamma^\mu p_\mu + m}{(p^0)^2 - \varepsilon^2 + i\epsilon} e^{-ip\cdot(x-x')} \\
= \int \frac{d^4p}{(2\pi)^4} & \frac{i}{\gamma^\mu p_\mu - m + i\epsilon} e^{-ip\cdot(x-x')} \ .
\end{aligned}
$$

Here the k-sum is replaced as Eq. (3.18), and for the ℓ-sum we use the following summation formula:

$$
\sum_{\ell=-\infty}^{\infty} e^{i(\ell+\nu)\theta} J_{\ell+\nu}(p_\perp r) e^{-i\ell\theta'} J_\ell(p_\perp r') = \left(\frac{re^{i\theta} - r'e^{i\theta'}}{|\boldsymbol{r} - \boldsymbol{r}'|} \right)^\nu J_\nu(p_\perp |\boldsymbol{r} - \boldsymbol{r}'|) \, . \qquad (3.22)
$$

For the ideal framework to analyze the rotational response to chiral condensate, we employ the Nambu–Jona-Lasinio model [7,8], which is an effective model including only the contribution of the leading order in the large N_c limit. In a rotating frame, this effective Lagrangian reads

$$
\mathcal{L}_{\mathrm{NJL}} = \bar{\psi}\, i\gamma^\mu (\partial_\mu + \Gamma_\mu)\psi + \frac{G}{2} \left[(\bar{\psi}\psi)^2 + (\bar{\psi}i\gamma_5\psi)^2 \right] \, . \qquad (3.23)
$$

At the one-loop order in the mean-field approximation, the effective thermodynamic potential at zero temperature is obtained by introducing the covariant derivative Γ_μ to Eq. (C.5) with $N_f = N_c = 1$, $m_0 = 0$ and $\beta \to \infty$:

$$
\Gamma_{\mathrm{eff}}[m(r)] = \frac{1}{V_4} \int d^4x \, \frac{m(r)^2}{2G} - \frac{1}{V_4} \operatorname{Tr} \ln \left[\partial_\mu + \Gamma_\mu - m(r) \right] \, , \qquad (3.24)
$$

where V_4 is the volume factor in four dimensional spacetime, i.e. $V_4 = \pi R^2 \times$(area of the tz-plan). Since rotation involves the centrifugal force, we here assume the thermodynamic potential with the inhomogeneity along the radial direction. We note that such an assumption is necessary even without rotation because the radial size of the cylindrical systems is finite. To determine the dynamical mass (or chiral condensate), we have to self-consistently solve the gap equation that corresponds to the optimization condition of the effective potential, $\delta\Gamma_{\mathrm{eff}}[m(r)]/\delta m(r) = 0$. For such a functional gap equation, however, it is technically difficult to find the exact solution [90]. In our analysis, we utilize the local density approximation; we suppose that the spatial fluctuation of the dynamical mass are negligible compared with the mass itself, namely, $\partial_r m \ll m^2$ [77]. Under this approximation, the Dirac operator can be diagonalized with the

complete set of the eigenfunctions $u_\pm(x)$ and $v_\pm(x)$, as well as in the homogeneous case. Then the effective potential in the local density approximation is obtained as the decomposed form of the vacuum part and the rotational part:

$$\Gamma_{\mathrm{eff}}[m(r)] = \frac{1}{V_4} \int d^4x \, \frac{m(r)^2}{2G} + \Gamma_0[m(r)] + \Gamma_\Omega[m(r)] \,, \tag{3.25}$$

with

$$\Gamma_0 = -\frac{1}{V_4} \int d^4x \sum_{\ell=-\infty}^{\infty} \sum_{k=1}^{\infty} \frac{J_\ell(p_{\ell,k}r)^2 + J_{\ell+1}(p_{\ell,k}r)^2}{\pi R^2 J_{\ell+1}(p_{\ell,k}R)^2} \\ \times \int_{-\infty}^{\infty} \frac{dp_z}{2\pi} \sqrt{p_z^2 + \varepsilon_{\mathrm{tr}}^2} \,, \tag{3.26}$$

$$\Gamma_\Omega = -\frac{1}{V_4} \int d^4x \sum_{\ell=-\infty}^{\infty} \sum_{k=1}^{\infty} \frac{J_\ell(p_{\ell,k}r)^2 + J_{\ell+1}(p_{\ell,k}r)^2}{\pi R^2 J_{\ell+1}(p_{\ell,k}R)^2} \, \theta\left(\Omega|\ell+1/2| - \varepsilon_{\mathrm{tr}}\right) \\ \times \int_{-q_{\ell,k}}^{q_{\ell,k}} \frac{dp_z}{2\pi} \left[\Omega|\ell+1/2| - \sqrt{p_z^2 + \varepsilon_{\mathrm{tr}}^2}\right] . \tag{3.27}$$

Here $q_{\ell,k} \equiv \sqrt{\Omega^2(\ell+1/2)^2 - p_{\ell,k}^2 - m(r)^2}$ is an effective Fermi momentum along the radial direction, and $\varepsilon_{\mathrm{tr}} = \sqrt{p_{\ell,k}^2 + m(r)^2}$ is the transverse energy. In the above expressions, the terms proportional to $J_\ell(p_{\ell,k}r)^2$ and $J_{\ell+1}(p_{\ell,k}r)^2$ correspond to the spin-up $(\ell_+ = \ell)$ and spin-down $(\ell_- = \ell + 1)$ modes, respectively. From the radial momentum discretization (3.14), we confirm that each ingredient in the momentum sum is unchanged under the replacement $\ell \leftrightarrow -\ell - 1$, or equivalently $j \leftrightarrow -j$. Therefore the contributions of fermions (the $j > 0$ states) and antifermions (the $j < 0$ states) are equivalently included in Γ_Ω, and rotation affects particle and antiparticle similarly. This is a big difference from the real density effect, which works to fermions and antifermions oppositely.

3.4 Rotation at zero temperture

Because of the step function in Γ_Ω, which originates from the zero-temperature distribution function with the effective chemical potential $\mu_\ell \equiv \Omega(\ell+1/2)$, only energy modes that satisfies $\varepsilon_{\mathrm{tr}} < \Omega|\ell+1/2|$ gives a rotational contribution. In the competition between $\Omega|\ell+1/2|$ and $\varepsilon_{\mathrm{tr}}$, it is quite crucial whether the cylinder radius is finite.

Let us first consider nonnegative ℓ modes with $m(r) = 0$. If we took the infinite volume limit, $R \to \infty$, the radial momentum could be continuous and there would exist a zero mode. In cylindrical systems with a finite radius, however, the energy dispersion has the nonzero lower bound as

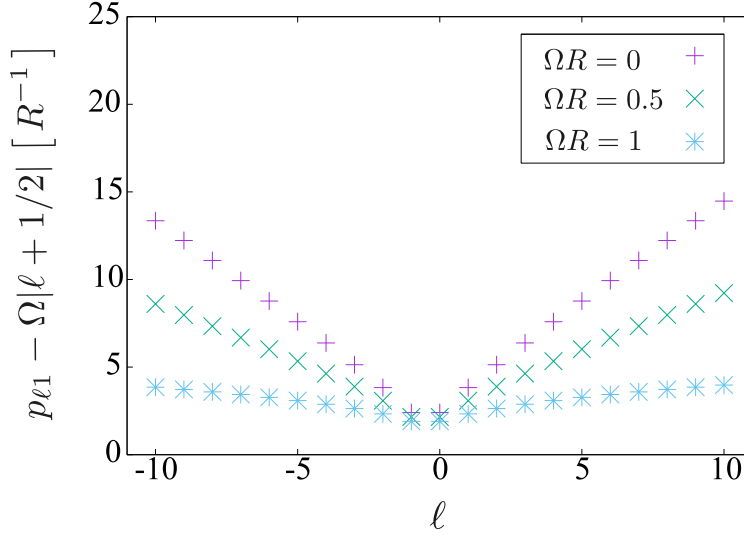$$\varepsilon_{\mathrm{tr}} = p_{\ell,k} \geq \xi_{\ell,1}/R > 0 \,. \tag{3.28}$$

Figure 3.2: Infrared dispersions of rotating fermions. Since $j = \ell + 1/2$ is a good quantum number, the spectra are symmetric with respect to $\ell = -1/2$, as shown in Eq. (3.14). The $\ell = 0$ (i.e. $j = 1/2$) and $\ell = -1$ (i.e. $j = -1/2$) mode are the lowest energy states.

From this relation we obtain

$$
\begin{aligned}
\varepsilon_{\mathrm{tr}} - \Omega|\ell + 1/2| &\geq \frac{1}{R}\Big[\xi_{\ell,1} - \Omega R(\ell + 1/2)\Big] \\
&\geq \frac{1}{R}\Big[\xi_{\ell,1} - (\ell + 1/2)\Big] > 0\,,
\end{aligned}
\tag{3.29}
$$

which follows from the property of the Bessel zero in Eq. (2.21). Similarly it can be checked that $\varepsilon_{\mathrm{tr}} > \Omega|\ell + 1/2|$ is true for arbitrary $\ell < 0$. In Figure 3.2, we plot the infrared spectra $p_{\ell 1} - \Omega|\ell + 1/2|$ as a function of l. Therefore regardless of the magnitude of angular velocity, rotation never contributes to the effective thermodynamic potential, which means $\Gamma_\Omega = 0$. We should emphasize again that this consequence results from the causality constraint $R\Omega \leq 1$ and the boundary effect leading to the infrared gap $\sim 1/R$.

To clarify the role of the boundary gap for rotation, it is worthwhile to refer the thermodynamics at finite density. In a system with finite chemical potential, microscopic quantities (e.g. the Dirac eigenvalue) should be modified even at zero temperature. This is not the case for macroscopic quantities. Because of the distribution function $\theta(\mu - \varepsilon)$, the density effects on thermodynamics never emerge at zero temperature unless the chemical potential is lager than the infrared threshold, i.e. fermion mass. In the finite-density QCD, this is known as the Silver Blaze problem [91]. We see a similar situation in rotating systems. It naïvely seems that rotation induces the alignment of the angular momentum. If so, chiral condensate with zero total angular momentum is no longer most favored. However the effective chemical potential $\Omega(\ell + 1/2)$ cannot exceed the infrared threshold $p_{\ell,k} = \xi_{\ell 1}/R$ (see Figure 3.3). Hence the rotational effect on chiral condensate is never realized at zero temperature, as we have discussed
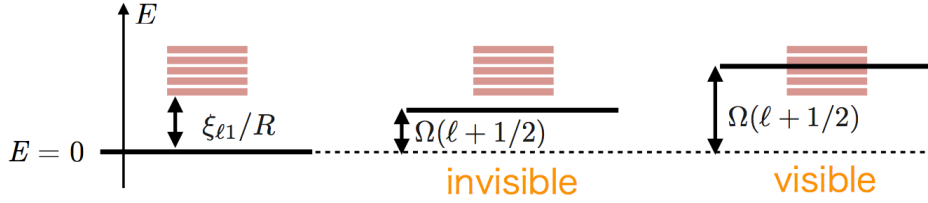
Figure 3.3: Schematic picture of the rotational effect on fermionic matter at zero temperature. In the finite-size cylinder with radius R, fermions possess the infrared energy gap (the left figure). If the number of occupied modes were changed for finite Ω, then rotation would affect thermodynamic quantities (the right figure). However, the effective chemical potential $\Omega(\ell + 1/2)$ never exceed the infrared energy gap $\xi_{\ell,1}/R$, no matter how large Ω is (the middle figure). Therefore the rotational effect does not appear at zero temperature. This is similar to the density case with a chemical potential smaller than the lowest energy gap i.e. the mass threshold.

above.

3.5 Dynamical mass at zero temperature

We discuss the chiral symmetry breaking in finite-size systems at zero temperature. Due to the absence of the rotational effect, the spatial profile of the dynamical mass is computed as the solution for the gap equation

$$\frac{m(r)}{G} = m(r) \int_{-\infty}^{\infty} \frac{dp_z}{2\pi} \sum_{\ell=-\infty}^{\infty} \sum_{k=1}^{\infty} \frac{f(p\,;\Lambda,\delta\Lambda)}{\pi R^2 J_{\ell+1}(p_{\ell,k}R)^2} \frac{J_\ell(p_{\ell,k}r)^2 + J_{\ell+1}(p_{\ell,k}r)^2}{\sqrt{p_{\ell,k}^2 + p_z^2 + m(r)^2}} \,, \tag{3.30}$$

which follows from $\delta\Gamma_0[m(r)]/\delta m(r) = 0$. Here to remove the ultraviolet divergence, we introduced the cutoff function

$$f(p\,;\Lambda,\delta\Lambda) = \frac{\sinh(\Lambda/\delta\Lambda)}{\cosh(p/\delta\Lambda) + \cosh(\Lambda/\delta\Lambda)} \tag{3.31}$$

with $p \equiv \sqrt{p_{\ell,k}^2 + p_z^2}$. In the numerical calculation, we adopt the parameters in Table 3.1. Here $G_c = 19.65\,\Lambda^{-2}$ is the critical value of G for $R \to \infty$ and $\delta\Lambda/\Lambda = 0.05$. For $\Lambda \simeq 1\,\mathrm{GeV}$ (the standard choice in QCD), the smaller radius in Table 3.1 corresponds to the typical radial scale of heavy ion; $R = 30\Lambda^{-1} \simeq 6\,\mathrm{fm}$.

We numerically solve Eq. (3.30) and show the r-dependence of its solution in Figure 3.4. In the region with small r, we see the plateau independent off the system size. On the other hand, as r grows there appears the boundary effect that suppresses the dynamical mass. The vanishing of the mass at $r = R$ results from the boundary condition (3.13). We note that
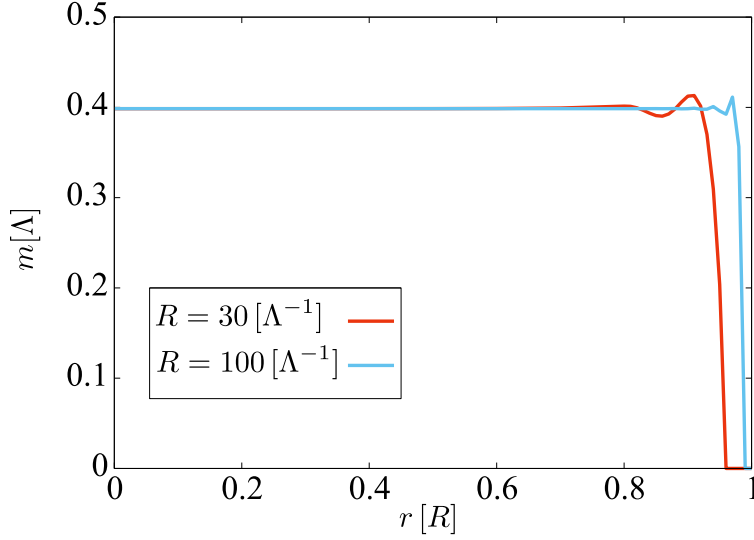
Figure 3.4: Inhomogeneous dynamical mass as a function of the radial coordinate r [80]. In the region expect for the vicinity of the boundary $r \simeq R$, the local density approximation is legitimate. At the boundary $r = R$, the mass should be zero because of the condition (3.13). For large R, the oscillation behavior becomes smaller, and it eventually disappears in the thermodynamic limit $R \to \infty$.

our analysis is valid only for not too large r because the local density approximation is valid only for $|\partial_r m| \ll m^2$. In Fig. 3.4, we also see that the dynamical mass has an oscillational behavior at $r \simeq 0.9R$, which is a cutoff artifact in the discrete sum of ℓ and k. Such an oscillation should completely disappear in the limit of $R \to \infty$ where the discrete sum becomes continuous. Indeed we confirm that the oscillation for $R = 100\Lambda^{-1}$ is smaller and comes closer to the boundary than the one for $R = 30\,\Lambda^{-1}$. Contrary to this, the boundary effect is generally enhanced for small R, as shown in Fig. 3.4. At the same time, the cutoff artifact in the ℓ- and k-sum becomes larger (more badly oscillating) because the spacing in discrete $p_{\ell,k}$ grows as R decreases. Furthermore although the magnitude of the dynamical mass is quite sensitive to the coupling G, the boundary effect is irrelevant to the coupling. From numerical calculation with different G, we have actually confirmed that the structures of the spatial profile, i.e. both the plateau at $0 \leq r \lesssim 0.8\,R$ and the oscillational behavior at $r \gtrsim 0.8R$ are unchanged even if G is

Table 3.1: Parameters in the numerical calculation for Eq. (3.30)

In Fig. 3.4	$R\,[\Lambda^{-1}]$	$G\,[G_c]$	$\delta\Lambda\,[\Lambda]$
red line	30	0.61	0.05
blue line	100	0.61	0.05

changed.

3.6 Environments affected by rotation

So far we have seen that rotation does not affect macroscopic (i.e. thermodynamic) quantities. This conclusion essentially stems from the fact that the physical scale of wave functions is characterized only by radius R, which cannot be greater than Ω^{-1} because of the causality constraint $R\Omega \leq 1$. Because of this, the infrared energy gap $(\sim R^{-1})$ is always larger than the rotational energy shift $(\sim \Omega)$. The situation should be changed, however, if other physical scale enters into theory. In other words, a parameter much stronger than R^{-1} enables us to neglect the boundary effect, and thus rotation can contribute to thermodynamics. In what follows, we see two possible situations where the rotational effect is visible.

Finite temperature

The first is the finite-temperature case. In this case, we employ the Fermi distribution function $\left[e^{\beta\{\varepsilon-\Omega(\ell+1/2)\}} + 1\right]^{-1}$ instead of $\theta\big(\Omega(\ell + 1/2) - \varepsilon\big)$, and then the rotational effect is visible even for $\varepsilon > \Omega(\ell + 1/2)$. Therefore, the dynamical mass is obtained as the solution for the following gap equation:

$$
\begin{aligned}
\frac{m(r)}{G} = m(r) \int_{-\infty}^{\infty} \frac{dp_z}{2\pi} \sum_{\ell=-\infty}^{\infty} \sum_{k=1}^{\infty} & \frac{1}{\pi R^2 J_{\ell+1}(p_{\ell,k}R)^2} \\
\times & \frac{J_\ell(p_{\ell,k}r)^2 + J_{\ell+1}(p_{\ell,k}r)^2}{\sqrt{p_{\ell,k}^2 + p_z^2 + m(r)^2}} \left[f(p\,;\Lambda,\delta\Lambda) - \frac{2}{e^{\beta\{\varepsilon-\Omega(\ell+1/2)\}} + 1} \right],
\end{aligned}
\tag{3.32}
$$

Here we should insert the cutoff function for the vacuum contribution, while the thermal contribution does not require it. The factor 2 of the Fermi distribution function comes from the fact that fermions and antifermions are not distinguished for the rotational effect.

In Figure 3.5, we plot the numerical solution for the above equation with $T = 0.2\Lambda$, $R = 30\Lambda^{-1}$, and G, $\delta\Lambda$ in Table 3.1. In Fig. 3.5 rotation leads to decreasing the dynamical mass for a fixed r. Thus we confirm that the rotational energy shift plays the role of an effective chemical potential. For a fixed Ω, the suppression becomes strong at large r. This stems from the enhancement of the centrifugal force for large r. The oscillations of the dynamical mass is the cutoff artifact same as that in Fig. 3.4. Indeed both in Figs. 3.4 and 3.5, such behaviors emerge at $r \simeq 0.9R$. For small Ω, the damping of the mass is not so large except for the vicinity of the boundary $r = R$. For example, for $\Omega R = 0.3$ (the blue line), we find that $|\partial_r m(r)|$ is less than 5% of $m^2(r)$ within $0 \leq r \lesssim 0.4R$. Therefore our analysis with the local density approximation is more reliable for small Ω. On the other hand, for $\Omega R = 0.5$ (the yellow line), the derivative terms of $m(r)$ should be taken into account. This is quite natural because the rotational effect with large Ω generates more intense inhomogeneity.
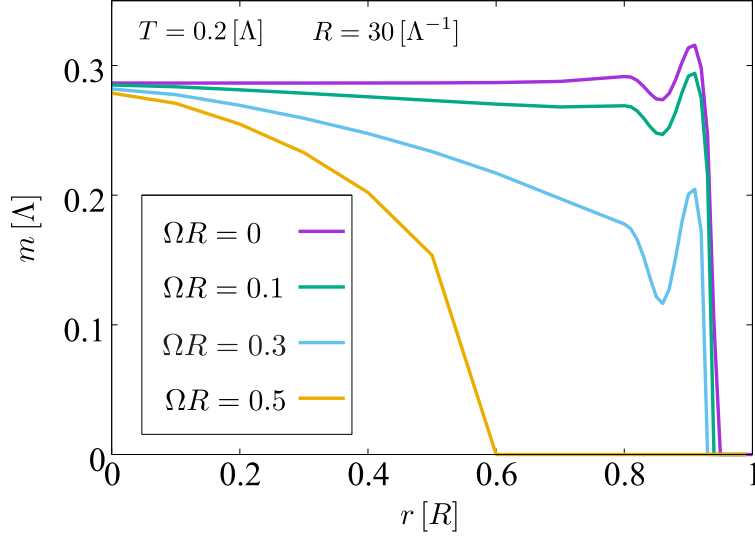
Figure 3.5: The rotational effect on the dynamical mass as the solution for Eq. (3.32). The dynamical mass is more suppressed when the effective chemical potential or angular momentum Ω becomes large. The oscillation at $r \simeq 0.9R$ is the cutoff artifact similar to that in the zero temperature calculation (see Fig. 3.4)

Besides, a rotating system at finite temperature is related to the recent topic of the QCD physics. Let us consider a high-temperature system with $T \gg R^{-1} \geq \Omega$. In such a case, the bulk constraint at the boundary is no longer relevant because of the thermal screening. In fact, for rotating right-handed fermions with small Ω, we analytically derive the following axial current:

$$\boldsymbol{j}_{\mathrm{A}}^{\mathrm{CVE}} = \frac{T^2 \boldsymbol{\Omega}}{12} + \frac{\Omega^2 \boldsymbol{\Omega}}{48\pi^2} + O(\Omega R^{-2}) \quad \text{for} \quad T \gg R^{-1} \geq \Omega \,, \tag{3.33}$$

which is originally discussed for the neutrino radiation in a rotating black hole [81–83]. Nowadays this current is investigated in the context of the transport phenomenon coupled with the vorticity generated in non-central heavy-ion collisions. The vorticity generated after the collision is evaluated as $\Omega \simeq 1\,\mathrm{MeV}$ [54], which is much smaller scale compared with the temperature $T \sim \Lambda_{\mathrm{QCD}}$. Therefore the vortex in the collisions satisfies $T \gg \Omega \geq R^{-1}$ with the vortex size R. The current generation by vortex in the heavy-ion collision is called the chiral vortical effect. An interesting aspect of the chiral vortical effect is that it is strongly connected to quantum anomaly. Independently of Ref. [81], the same expression is obtained with the gauge-gravity duality [92, 93]. and then it is discussed that the coefficient of the current is yielded by the chiral anomaly coupled with Riemann tensors. However, this seems a contradiction with the current calculated in rotating frames, which has zero Riemann tensor. Hence we should clarify how the anomalous aspect of the chiral vortical current is extracted from the Dirac field theory in rotating frames [94].
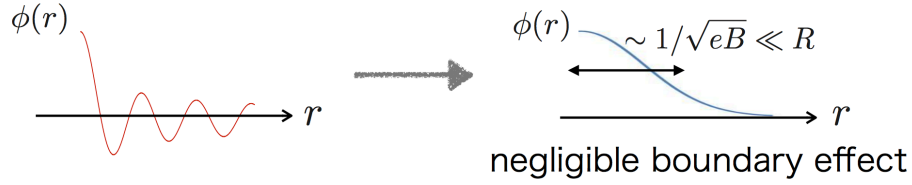
Figure 3.6: Difference between the radial parts of the wave function without/with magnetic field. In general, the Bessel function does not converge even at infinity (although it is known that $J_\ell(z) \sim 1/z$ for $z \gg |\ell^2 - 1/4|$ [95]). On the other hand, the Landau wave function is localized with the width characterized by the magnetic length $\ell_B = 1/\sqrt{eB}$. If magnetic field is quite large as $\ell_B \ll R$, hence, magnetized fermionic matter is affected by rotation even at zero temperature.

Magnetic field

The second environment that rotation affects is magnetized systems. Under a strong magnetic field, the Landau wave-function is localized with the length scale $\sim \ell_B = 1/\sqrt{eB}$ (see Figure 3.6). If this wave function is much squeezed than system size, i.e. $\sqrt{eB} \gg R^{-1}$, then the boundary effects are essentially irrelevant to dynamics. Also in this case, the radial momentum is characterized by the Landau level, which is independent of angular momentum. This is different from the rotating systems without magnetic field, where the radial momentum depends on ℓ, as we have seen in Eq. (3.14). Therefore there always exist exited modes that exceed the effective chemical potential. Namely a strong magnetic field supports the rotational effect to be visible even at zero temperature. Following this argument, in Chapter 4 we discuss the magnetic response of the dynamical mass in a rotating system.

Intriguingly the magnetized rotating systems are also related to an anomalous phenomenon, as well as the rotating system at finite temperature. We know that a strong magnetic background triggers intriguing transport phenomena involving a $\mathcal{P}$- and $\mathcal{CP}$-odd current and density [55–58, 96–99] (see also Refs. [51, 59, 100, 101]). From the viewpoint of the analogy between density and rotation, such phenomena are expected to take place in rotating magnetized systems. Indeed we can analytically obtain the anomalous number density as

$$n_{\text{total}} = \frac{eB\Omega}{4\pi^2}(N + 1) \,, \tag{3.34}$$

where $N = \lfloor eBR^2/2 \rfloor$ is the Landau degeneracy factor. In Refs. [78, 102], the similar relation to Eq. (3.34) is derived. However their anomalous density picks up only the second term, which corresponds to the spin part. If we employ the thermodynamic potential in magnetized rotating systems, it is concluded that the total angular momentum (i.e., both the orbital and spin angular momentum) contribute this anomalous effect (see Section 4.3).

We note that the above induced density comes from the imbalance of the contributions of fermions and antifermions. In other words, magnetic field creates an energetically favored

modulus of the total angular momentum for rotating charged particle. Indeed, if magnetic field is not applied, rotation does not distinguishes $j > 0$ and $j < 0$ modes, as seen in Eq. (3.26), and thus the number density should be zero. Also rotation is necessary for the density because particles with $j > 0$ and antiparticle with $j < 0$ has same energy dispersions only with magnetic field.

Finally we again stress the analysis of the rotational effect becomes complicated if external sources are not much stronger than the scale of energy gap $\sim R^{-1}$. In such cases, we properly take into account the boundary effect, as we have done for solving Eq. (3.32). Then there appears an infrared energy gap, which plays the essential role to determine the dynamics of rotating fermions. Fortunately, this is not the case in most QCD systems of interest: $T \gg R^{-1}$ in a quark-gluon plasma or $\sqrt{eB} \gg R^{-1}$ in a neutron star. However for an applications to table-top experiments, more precise treatment of the boundary effect would be important.

Chapter 4

Chiral symmetry with rotation and magnetic field

Magnetic field is a useful probe for various intriguing phenomena in QCD since many systems with a gigantic magnetic field could be realized; the early unverse [21–23], compact stars [24], and heavy-ion collision experiments [25–27]. Especially a magnetic field produces the complicated but rich chiral structure. In this chapter, we discuss the rotating and magnetized fermionic system. After constructing the fundamental framework, we investigate the rotational effect on chiral symmetry. Then we obtain the inverse phenomenon of the magnetic catalysis induced by rotation, which we term the rotational magnetic inhibition.

4.1 Magnetic response of chiral condensate

Magnetic catalysis

Before our discussion of the rotational effects on the dynamical symmetry breaking, we see an intuitive picture of the magnetic catalysis. Let us focus on the fermionic modes with zero angular momentum. Namely we only consider the condensate of the paired state with zero total orbital angular momentum ($L_{\rm tot} = 0$). Since chiral condensate is a scalar condensate, which has zero total angular momentum ($J_{\rm tot} = 0$), it should be constructed by fermion and antifermion with opposite individual spins so that the total spin can be zero ($S_{\rm tot} = 0$). In the magnetized system, the spin of a positive-charged (negative-charged) particle tends to be aligned parallelly (antiparallelly) to magnetic field (see Figure 4.1). Therefore such a paired state is energetically stable under a magnetic field, and its condensation is enhanced by the magnetic field.

In order to understand more precisely how magnetic field affects chiral condensate or the dynamical mass, let us see the infrared energy spectra for magnetized fermions [36]. In a strong
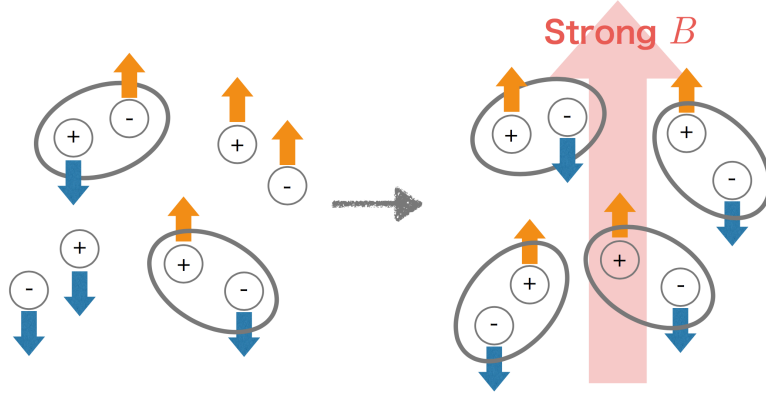
Figure 4.1: Schematic figure for chiral condensate in a strong magnetic field. Each arrow of a charged particle denotes the direction of its spin. Chiral condensate can be formed by particles with oppositely aligned spins. The number of the possible paired state increases due to the Zeeman flip.

magnetic field, the dispersion of fermions is discretized as

$$E_{3+1\text{D}} = \sqrt{eB(2n + 1 - 2s_z) + p_z^2 + m^2}\,,\tag{4.1}$$

where the integer n runs from zero to infinity. It is clear that the lowest mode $n = 0$ dominates in the strong eB limit. Namely the dynamics is described only by spin-up fermions with the effective $1+1$-dimensional spectrum: $E_{1+1\text{D}} = \sqrt{p_z^2 + m^2}$. In the NJL model with an attractive interaction, such a reduction of dimension leads to the following equation for the dynamical mass:

$$\frac{1}{G} = \frac{eB}{2\pi} \sum_{n=0}^{\infty} \alpha_n \int_0^\Lambda \frac{dp_z}{2\pi} \frac{1}{\sqrt{2neB + p_z^2 + m^2}} \simeq \frac{eB}{2\pi} \int_0^\Lambda \frac{dp_z}{2\pi} \frac{1}{\sqrt{p_z^2 + m^2}}\,,\tag{4.2}$$

with $\alpha_n = 2 - \delta_{n0}$. This is the magnetized version of Eq. (C.10) with $N_c = N_f = 1$. We shall revisit Eq. (4.2) later (although the regularization scheme is different). The solution is analytically obtained as

$$m \sim \Lambda \exp\left[-\frac{(2\pi)^2}{GeB}\right]\,,\tag{4.3}$$

which exponentially increase as eB increases. The above solution shows that the dynamical symmetry breaking is realized even for an infinitesimally small interaction. From the viewpoint of the analogy to superconductivity, this is nothing but the Cooper instability. Indeed in the Bardeen–Cooper–Schrieffer theory, the superconducting energy-gap Δ is determined from the following gap equation:

$$\frac{1}{G} = \rho(0) \int_0^{\hbar\omega_{\text{D}}} \frac{d\varepsilon}{\sqrt{\varepsilon^2 + \Delta^2}}\,.\tag{4.4}$$

where $\rho(0)$ denotes the density of states on the Fermi surface, and ω_{D} represents the Debye
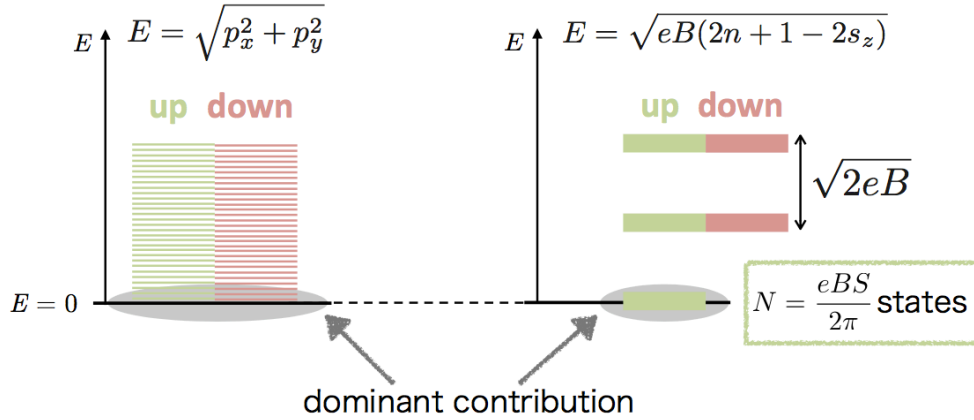
Figure 4.2: Spectrum without/with magnetic field. The Landau degeneracy amplifies the dominant contribution for the dynamical mass generation.

frequency. Since this is mathematically equivalent to Eq. (4.2), the solution is readily given by

$$\Delta \sim \hbar \omega_{\mathrm{D}} \exp\left[-\frac{1}{G\rho(0)}\right] . \tag{4.5}$$

Thus the Cooper instability is realized due to the finite density of states on the Fermi surface; the gap is vanished for $\rho(0) = 0$. On the other hand in Eq. (4.2), $eB/2\pi$ plays the role of the density of states. Indeed this coefficient is the Landau degeneracy factor, which corresponds to the density of states for the lowest Landau level $n = 0$. Therefore the essential concept of the magnetic catalysis is that the density of states for the infrared mode becomes finite due to the Landau quantization (see Figure 4.2).

Inverse magnetic catalysis

In finite-density systems, the magnetic response is drastically changed; magnetic field decreases chiral condensate, and eventually restores chiral symmetry, which is named the inverse magnetic catalysis. This phenomenon is understood as follows. For simplicity, we see the zero temperature case. The thermodynamic potential at finite chemical potential μ is decomposed into the vacuum and density contribution, as well as the one at finite angular velocity, Eq. (3.27). Namely the dynamical mass is determined by the competition between these two. The density contribution comes from the prohibition of the low energy excitation due to the shift of the Fermi surface (see Figure 3.3). The strength of the density contribution is thus characterized by the volume of Fermi sphere. Without magnetic field, this volume is typically obtained as

$$\int_{|\boldsymbol{p}|<\mu} d^3p \sim \mu^3 . \tag{4.6}$$

On the other hand, since only the lowest Landau level survives in strong magnetic fields, the
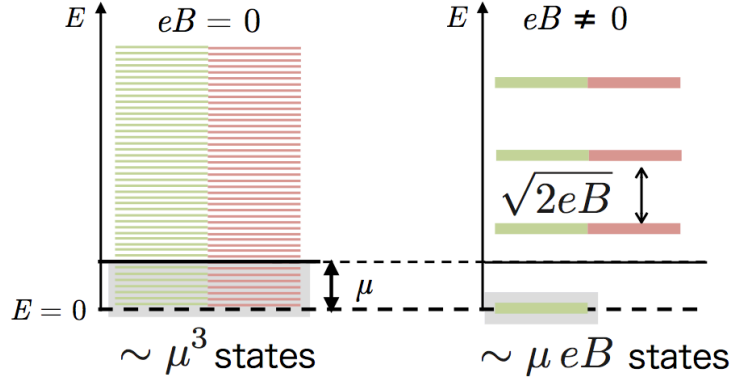
Figure 4.3: Density effect without/with magnetic field. Shaded parts represents the modes that cannot be excited. Because of the Landau degenerate, more modes cannot be exited in a strong magnetic field, and thus the dynamical mass is suppressed as magnetic field increases.

phase space becomes

$$\frac{eB}{2\pi} \int_{-\mu}^{\mu} dp \sim \mu\, eB\,. \tag{4.7}$$

We find for $eB \gtrsim \mu^2$, the density contribution with magnetic field is larger than that without magnetic field (see Figure 4.3). In other word, the dynamical mass is more suppressed because of a strong magnetic field. In fact, the results from the NJL model or the holographic QCD agree that the inverse magnetic catalysis becomes visible for $\mu \sim \sqrt{eB}$ [41]. Here we note that the vacuum contribution is also changed by magnetic field. For this reason, the actual vacuum structure with magnetic field and density is determined more complicatedly. For exmaple, the dynamical mass oscillates as a function of eB/μ^2, which is called the de Haas-van Alphen oscillation [103, 104]. Even from the above simple argument, however, we find that the density of states for the lowest Landau mode plays the crucial role to lead to the inverse magnetic catalysis, as well as magnetic catalysis. The analogy between density and rotation implies a possibility that rotation induces a similar phenomenon to the inverse magnetic catalysis. In this chapter, we discuss the magnetic response of the chiral condensate in rotating systems, and obtain such a novel phenomenon, i.e. the rotational magnetic inhibition.

4.2   Dirac equation

We first find the energy dispersion of rotating fermions interacting with magnetic fields. In the presence of gauge field, the modification of the Dirac theory in curved spacetime is replacing ∂_μ with the covariant derivative $D_\mu = \partial_\mu + ieA_\mu$. Then the Dirac equation (3.3) is changed into

$$\big[i\gamma^\mu(D_\mu + \Gamma_\mu) - m\big]\psi = 0\,, \tag{4.8}$$

and the definition of γ^μ and Γ_μ are the same as without gauge field. We consider the system with the constant magnetic field parallel to the rotation axis; $\boldsymbol{B} = B\hat{z}$ and $\boldsymbol{\Omega} = \Omega\hat{z}$. This

corresponds to the system depicted in Fig. 2.1 under the background magnetic field. Let us choose the symmetric gauge in the inertial frame as $A_i = (0, By/2, -Bx/2, 0)$. The above Dirac equation is reduced into

$$
\begin{aligned}
\Bigg[i\gamma^0 &\left\{ \partial_0 - \Omega \left(x\partial_2 - y\partial_1 + \frac{i}{2}\sigma^{12} \right) \right\} \\
&+ i\gamma^1 \left(\partial_1 + i\frac{eBy}{2} \right) + i\gamma^2 \left(\partial_2 - i\frac{eBx}{2} \right) + i\gamma^3\partial_3 - m \Bigg] \psi = 0 \,.
\end{aligned}
\tag{4.9}
$$

The linear term of Ω here appears as effective chemical potential, as well as without magnetic field, Eq. (3.6). Solving the above Dirac equation, the energy dispersion for $eB > 0$ is obtained as

$$
\left[E + \Omega(\ell + s_z) \right]^2 = p_z^2 + (2n + 1 - 2s_z)eB + m^2 \,.
\tag{4.10}
$$

where ℓ and s_z denote the eigenvalues for L_z and S_z, respectively. If we realize that $E + \Omega(\ell + s_z)$ as the energy eigenvalue in the inertial frame, this can be obtained from the ordinary dispersion for the charged spin-s particle coupled with an external magnetic field, i.e.

$$
E^2 = p_z^2 + (2n + 1 - 2s_z)eB + m^2 \,.
\tag{4.11}
$$

We also obtain the eigenfunction for Eq. (4.9) as explained in Appendix A.2, but only the energy spectrum is sufficient in our discussion about the dynamical symmetry breaking. In what follows we discuss several features of magnetized Dirac fermions in rotating frames.

(I) Lorentz force in rotating frame

The gauge field in rotating frames, $A^\mu = A^i e_i^\mu$, leads to an electric field

$$
e\boldsymbol{E} = -e\,\boldsymbol{\nabla}A^t = -e\,\boldsymbol{\nabla}(-B\Omega r^2/2) = eB\Omega(x, y, 0) \,.
\tag{4.12}
$$

This is identified as the Lorentz force induced by rotation because the velocity vector at $(x, y, 0)$ caused by rotation is $\boldsymbol{v} = \boldsymbol{\Omega} \times \boldsymbol{x} = \Omega(x, y, 0)$. However, there appears no coupling term between rotation and magnetic field in Eq. (4.9) because the gamma matrix $\gamma^t = \gamma^i e_i^t$ cancels it out. Therefore rotation never induce any electromagnetic effect. In this point, we see the analogy between rotation and density.

(II) Momentum phase space

Let us focus on the motion in the xy-plane. In the ordinary Landau quantization, the energy level is designated only by an integer n instead of (p_x, p_y), as seen in Eq. (4.11). Namely one degree of freedom that characterizes the motion in the xy-plane disappears here, and each Landau level is degenerate with the Landau degeneracy factor given by

$$
N = \left\lfloor \frac{eBS}{2\pi} \right\rfloor \,,
\tag{4.13}
$$

where S is the area of the xy-plane. This factor N is gauge-independent, but the degree of freedom that gives the Landau degeneracy is different for each specific gauge choice. In the cylindrical coordinates, for example, the degenerate quantum number is the canonical angular momentum ℓ, and thus it should take N different integer. As explained in Appendix B, the Landau quantization imposes the lower bound of ℓ as $\ell \geq -n$. For the nth Landau level, hence, the possible range of ℓ should be

$$- n \leq \ell \leq N - n . \tag{4.14}$$

(Here we implicitly assume $N \gg 1$ with sufficiently strong magnetic field.) This possible range holds even for ℓ in Eq. (4.10), as shown in Appendix B. Therefore the spectrum in Eq. (4.10) is not degenerate. The integration in the $p_x p_y$-space becomes the double sum with respect to n and ℓ. For instance, for spin-1/2 fermions with up spin, we should rewrite the phase space sum into

$$\text{Magnetic field + Rotation:} \quad \int \frac{dp_x dp_y}{(2\pi)^2} \, \mathcal{I}(p_x, p_y) \to \frac{1}{S} \sum_{n=0}^{\infty} \sum_{\ell=-n}^{N-n} \mathcal{I}(n, \ell) . \tag{4.15}$$

If the function $\mathcal{I}$ is independent of ℓ, the phase space sum is reduced to the well-known form in a magnetic field:

$$\text{Magnetic field:} \quad \int \frac{dp_x dp_y}{(2\pi)^2} \, \mathcal{I}(p_x, p_y) \to \frac{1}{S} \sum_{n=0}^{\infty} \sum_{\ell=-n}^{N-n} \mathcal{I}(n) = \frac{eB}{2\pi} \sum_{n=0}^{\infty} \mathcal{I}(n) . \tag{4.16}$$

(III) Necessary condition for the Landau quantization in rotating frames

For quantization in harmonic oscillators, the system size should be large enough as compared to typical scales of the problem. Thus to realize the Landau quantization, which is mathematically the same as the one in harmonic oscillators, the system size scale should be larger than the magnetic length, namely $R \gg l_B = 1/\sqrt{eB}$ in the cylindrical systems (see Appendix A.2). Without rotation, the thermodynamic limit, i.e. $R \to \infty$ can always be taken validly. In rotating frames, however, we cannot consider systems with infinitely large radius because of the causality constraint $R \leq 1/\Omega$ [105, 106]. Therefore, our discussion about the Landau quantization in rotating frames is legitimate only if the following condition is imposed:

$$1/\sqrt{eB} \ll R \leq 1/\Omega . \tag{4.17}$$

We note that $N \gg 1$ follows from the above condition.

(IV) Realization of zero-modes

The Landau quantization drastically changes the structure of the energy spectrum of rotating fermions. The dispersion (4.10) shows that there exist the Landau zero modes $n = 0$
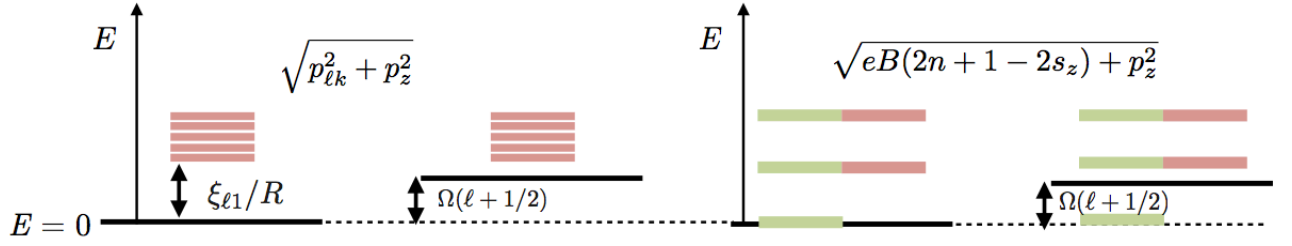
Figure 4.4: Rotational effect without/with magnetic field. In the case without magnetic field, the infrared energy gap always exceed the effective chemical potential, and thus the rotational effect is invisible at zero temperature. On the other hand, the Landau quantization enables rotating fermions to take the zero mode that is independent off angular momentum ℓ. Therefore rotation affect magnetized fermionic systems even at zero temperature.

independent of the angular momentum ℓ. Such lowest modes always receives the rotational effect (see Figure 4.4). Thus, the strongly magnetized fermionic matter should be affected by rotation even at zero temperature.

4.3 NJL model

To study the vacuum structure in the presence of rotation and magnetic field, we analyze the NJL model defined by

$$\mathcal{L}_{\mathrm{NJL}} = \bar{\psi}\, i\gamma^\mu (D_\mu + \Gamma_\mu)\psi + \frac{G}{2}\left[(\bar{\psi}\psi)^2 + (\bar{\psi}\gamma_5\psi)^2\right]. \tag{4.18}$$

Let us suppose that chiral condensate is homogeneous in the current setup (we shall briefly discuss about the validity of this assumption later). In the mean field approximation, the effective thermodynamic potential is obtained in the same manner for Eq. (C.5):

$$
\begin{aligned}
\Gamma_{\mathrm{eff}}(m) = \frac{m^2}{2G} - \frac{1}{\beta S}\int_{-\infty}^{\infty}\frac{dp_z}{2\pi}\sum_{n,\ell,s_z} \\
\times \left\{\frac{\beta\varepsilon}{2} + \ln\left[1 + e^{-\beta\left\{\varepsilon - \Omega(\ell + s_z)\right\}}\right] + \ln\left[1 + e^{-\beta\left\{\varepsilon + \Omega(\ell + s_z)\right\}}\right]\right\}.
\end{aligned}
\tag{4.19}
$$

Here we note that the number density (3.34) is derived from the above potential. To confirm this, we replace $\Omega(\ell + s_z)$ with $\Omega(\ell + s_z) + \mu$. For $T = m = 0$, the derivative $\partial\Gamma_{\mathrm{eff}}/\partial\mu$ in the lowest Landau approximation gives the following number density:

$$n_{\mathrm{total}} \simeq \frac{\Omega}{\pi^2 R^2}\sum_{\ell=0}^{N}(\ell + 1/2) = \frac{eB\Omega}{4\pi^2}(N + 1). \tag{4.20}$$

It is obvious that the first and second term are the contribution of orbital angular momentum and spin, respectively. Thus the total angular momentum affects this anomalous density, as we have mentioned in Section 3.6.

Now we return to the analysis of the dynamical symmetry breaking. Similarly to the case without magnetic field, at zero temperature this can be decomposed into the pure-magnetic and rotational contributions:

$$\Gamma_{\text{eff}}(m) = \frac{m^2}{2G} + \Gamma_0(m) + \Gamma_\Omega(m) \ , \tag{4.21}$$

with

$$\Gamma_0 = -\frac{eB}{2\pi} \sum_{n=0}^{\infty} \alpha_n \int_{-\infty}^{\infty} \frac{dp_z}{2\pi} \sqrt{p_z^2 + \varepsilon_{\text{tr}}^2} \ , \tag{4.22}$$

$$\Gamma_\Omega = -\frac{1}{S} \sum_{n=0}^{\infty} \alpha_n \sum_{\ell=-n}^{N-n} \theta(\Omega|\ell + 1/2| - \varepsilon_{\text{tr}}) \tag{4.23}$$
$$\times \int_{-q_{\ell,n}}^{q_{\ell,n}} \frac{dp_z}{2\pi} \left[\Omega|\ell + 1/2| - \sqrt{p_z^2 + \varepsilon_{\text{tr}}^2} \right] .$$

where $\varepsilon_{\text{tr}}^2 = 2neB + m^2$, and $q_{\ell,n} \equiv \sqrt{\Omega^2(\ell + 1/2)^2 - \varepsilon_{\text{tr}}^2}$. Here $\alpha_n = 2 - \delta_{n0}$ stems from the sum with respect to spin: only the up-spin mode can be the lowest Landau level, as seen in Eqs. (4.10) and (4.11). We note that Γ_Ω corresponds to the counterpart of the density contribution: if an effective chemical potential $\Omega|\ell + 1/2|$ is replaced with an actual chemical potential μ, the thermodynamic potential Γ_{eff} is same the one in finite-density systems.

To regularize the ultraviolet momentum in the effective thermodynamic potential (4.21), we adopt the same cutoff function as without magnetic field, namely,

$$f(p; \Lambda, \delta\Lambda) = \frac{\sinh(\Lambda/\delta\Lambda)}{\cosh(p/\delta\Lambda) + \cosh(\Lambda/\delta\Lambda)} \tag{4.24}$$

with $p \equiv \sqrt{p_z^2 + 2neB}$. Since a naïve cutoff function actually breaks the gauge transformation, the proper-time method [107] and the Pauli-Villars regularization are usually utilized for the usual magnetized NJL model. For instance, in the derivations of the magnetic catalysis in Refs. [28, 29], the proper-time method is used to regularize the pure-magnetic potential (4.22). It is known however that such a naïve cutoff scheme could give a qualitatively correct result as long as the parameter $\delta\Lambda$ is not too small [108]. Also the ultraviolet divergent structure is the same even if rotation is induced except for the ℓ-sum. For these reasons, $f(p; \Lambda, \delta\Lambda)$ should lead to results that physically make sense in our analysis.

The condition to minimize the effective potential, $\partial\Gamma_{\text{eff}}/\partial m = 0$, leads to the gap equation:

$$\frac{m}{G} = \frac{m}{\pi} \left(F_0 - F_\Omega \right) , \tag{4.25}$$

where the pure-magnetic term and the rotational term are respectively given by

$$F_0 \equiv \frac{eB}{2\pi} \sum_{n=0}^{\infty} \alpha_n \int_0^{\infty} \frac{dp_z \, f(p; \Lambda, \delta\Lambda)}{\sqrt{p_z^2 + \varepsilon_{\text{tr}}^2}} \ , \tag{4.26}$$

$$F_\Omega \equiv \frac{1}{S} \sum_{n=0}^{\infty} \alpha_n \sum_{\ell=-n}^{N-n} \theta(\Omega|\ell + 1/2| - \varepsilon_{\text{tr}}) \int_0^{q_{\ell,n}} \frac{dp_z \, f(p; \Lambda, \delta\Lambda)}{\sqrt{p_z^2 + \varepsilon_{\text{tr}}^2}} \ . \tag{4.27}$$

We note that F_Ω can be reduced to a simpler form if $q_{\ell,n}$ is negligibly small compared with Λ and $\sqrt{eB}$ (fortunately, this is the case for our analysis with a small G in Section 4.4). In this case, since the p_z-integral is irrelevant to the ultraviolet divergence, the cutoff function in F_Ω can be replace with $f(\sqrt{2neB}; \Lambda, \delta\Lambda)$. Such a simplification is a significant advantage for the analytical investigation: after the p_z-integral, Eq. (4.27) is then reduced to

$$F_\Omega \simeq \frac{1}{S} \sum_{n=0}^{\infty} \alpha_n \sum_{\ell=-n}^{N-n} \theta(\Omega|\ell + 1/2| - \varepsilon_{\mathrm{tr}}) \, f(\sqrt{2neB}; \Lambda, \delta\Lambda)$$
$$\times \ln\left(\frac{\Omega|\ell + 1/2| + \sqrt{\Omega^2(\ell + 1/2)^2 - \varepsilon_{\mathrm{tr}}^2}}{\varepsilon_{\mathrm{tr}}} \right) . \tag{4.28}$$

Instead of Eq. (4.25), in finite-density systems, the dynamical mass is determined from

$$\frac{m}{G} = \frac{m}{\pi}\left(F_0 - F_\mu \right) \tag{4.29}$$

with

$$F_\mu = \frac{eB}{2\pi} \sum_{n=0}^{\infty} \alpha_n \, \theta(|\mu| - \varepsilon_{\mathrm{tr}}) \ln\left(\frac{|\mu| + \sqrt{\mu^2 - \varepsilon_{\mathrm{tr}}^2}}{\varepsilon_{\mathrm{tr}}} \right) , \tag{4.30}$$

which is the same as F_Ω under the replacement $\Omega(\ell + 1/2) \to \mu$. Since the step function $\theta(|\mu| - \varepsilon_{\mathrm{tr}})$ truncates the sum in terms of n, an ultraviolet regularization is unnecessary for F_μ. Namely the density effects on chiral condensate comes only from the infrared physics. This implies that F_Ω is also not really sensitive to the regularization scheme if S is large enough.

We comment about the inhomogeneity of chiral condensate. Regardless whether chiral condensate is homogeneous or inhomogeneous, the dynamical mass is obtained from the gap equation

$$m = G \operatorname{tr}[S(x,x)] , \tag{4.31}$$

which is a general form of Eq. (4.25). From this equation, it is self-consistently verified that m should also be homogeneous if the Dirac propagator $S(x,y)$ is homogeneous. Under the condition (4.17), the eigenfunction for Eq. (4.9) is the same as without rotation (i.e the Landau wave function), as shown in Appendix A.2. Since this eigenfunction leads to the spatially homogeneous Dirac propagator, the mass in the local density approximation has no spatial dependence, unlike that without magnetic field. As the same time, there is no inhomogeneity in the thermodynamic potential, which is determined by the dynamical mass.

Within the above setup, we investigate the magnetic response for the dynamical symmetry breaking in rotating frames. In the finite-density NJL model coupled with magnetic field, we obtain the magnetic catalysis for a weak coupling ($G < G_c$) and the inverse magnetic catalysis for a strong coupling ($G > G_c$), where G_c is the critical coupling for the onset of the chiral condensate in the vacuum (i.e. $\Omega = \sqrt{eB} = 0$). Following the discussion in finite-density systems, we calculate the dynamical mass in these two cases. Although the former is not a practical case, this is convenient to confirm the analogy between density and rotation. The

numerical calculation is performed with the parameters in Table 4.1. It is easily checked that eB, R and Ω in these choices satisfy Eq. (4.17) so that the analysis based on the Landau quantization in a rotating frame is justified. We have numerically confirmed that $\delta\Lambda$ is qualitatively irrelevant to our results.

4.4 Dynamical mass for weak coupling

Let us discuss the weak coupling case. The numerical results are shown in dimensionless unit in terms of

$$m_{\mathrm{dyn}} = 1.25 \times 10^{-2}\,\Lambda \, , \tag{4.32}$$

which is the solution of the gap equation with $eB = 0.2\,\Lambda^2$ and $\Omega = 0$. We plot Figure 4.5, where the red line corresponds to the solution for Eq. (4.25) as a function of Ω. The horizontal axis represents an effective chemical potential

$$\mu_N \equiv \Omega N \, . \tag{4.33}$$

Also in Fig. 4.5, the blue line is the solution for Eq. (4.29) with $\mu = \mu_N$. From the comparison between Eqs. (4.28) and (4.30), we find that this $\mu_N = \Omega N$ is the maximum counterpart of μ. Figure 4.6 is a 3D plot for the solution of Eq. (4.25) as a function of Ω and eB. From this 3D plot, we can calculate the critical value Ω_c (i.e. the onset value of of angular velocity for chiral symmetry breaking), which is plotted as a function of magnetic field in Figure 4.7. Here are some remarks on these numerical results.

(I) Comparison between density and rotation

When the angular velocity exceeds $\Omega \simeq m_{\mathrm{dyn}}/N$, the rotational effects become visible with the smooth damping of the dynamical mass (see the red line in Fig. 4.5). On the other hand, the density effect appears as the sharp damping of the dynamical mass, and thus this is the first order phase transition (see the blue line in Fig. 4.5). Such a difference is understood from the viewpoint of the number of relevant modes to the suppression. Let us focus only on the lowest Landau level $n = 0$ (although the following argument is also applicable even including

Table 4.1: Parameters in the numerical calculations for Eqs. (4.25) and (4.29). Here G_c is the critical coupling obtained with $\Omega = \sqrt{eB} = 0$ and $\delta\Lambda = 0.05\,\Lambda$.

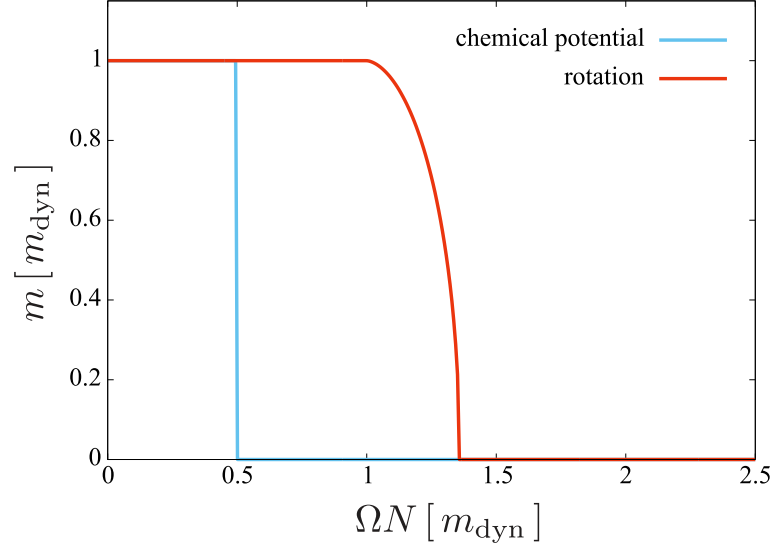|	$G\,[G_c]$	$\Omega\,[\Lambda]$	$eB\,[\Lambda^2]$	$R\,[\Lambda^{-1}]$	$\delta\Lambda\,[\Lambda]$
Weak coupling	0.62	$0 - 2 \times 10^{-7}$	$0.01 - 0.02$	10^3	0.05
Strong coupling	1.11	$0 - 10^{-5}$	$0.1 - 0.2$	10^3	0.05

Figure 4.5: Dynamical mass for $eB = 0.2\,\Lambda^2$ as the solution for Eq. (4.25) (red line) and Eq. (4.29) with $\mu = \mu_N$ (blue line) [76].

higher Landau levels); for F_Ω and F_μ with the parameter in Table 4.1 the lowest Landau level approximation is valid. Because of the step function in F_Ω, only the modes with $\ell > m/\Omega - 1/2$ are relevant. Indeed the red line in Fig. 4.5 begins decreasing at $N\Omega = m_{\mathrm{dyn}}$, which corresponds to the threshold that F_Ω becomes finite. On the other hand, the step function in F_μ says that all N modes simultaneously start contributing for $\mu > m$. As a result, the finite-density effect arises suddenly when μ exceeds a critical value.

For the comparison between the red and the blue lines in Fig. 4.5, it is useful to approximate the ℓ-sum as an integration. Suppose that Ω is small enough to treat $\Omega(\ell + 1/2)$ as a continuous variable. Since N is a sufficiently large integer ($N \sim \mathcal{O}(10^4)$ in Table 4.1), the ℓ-sum in F_Ω can be represented as

$$\sum_{\ell=-n}^{N-n} \ln\left(\frac{\Omega|\ell + 1/2| + \sqrt{\Omega^2(\ell + 1/2)^2 - \varepsilon_{\mathrm{tr}}^2}}{\varepsilon_{\mathrm{tr}}}\right) \theta(\Omega|\ell + 1/2| - \varepsilon_{\mathrm{tr}})$$
$$\simeq \frac{1}{\Omega} \int_0^{\mu_N} d\mu \ln\left(\frac{\mu + \sqrt{\mu^2 - \varepsilon_{\mathrm{tr}}^2}}{\varepsilon_{\mathrm{tr}}}\right) \theta(\mu - \varepsilon_{\mathrm{tr}}) . \tag{4.34}$$

This means that the rotational contribution in Eq. (4.25) is reduced to

$$F_\Omega = F_\mu(\mu = \mu_N) - \frac{eB}{2\pi} \sum_{n=0}^{\infty} \alpha_n \sqrt{1 - \frac{\varepsilon_{\mathrm{tr}}^2}{\mu_N^2}} \, \theta(\mu_N - \varepsilon_{\mathrm{tr}}) . \tag{4.35}$$

Namely the rotational contribution F_Ω has the density-like effect as the first term F_μ. The second term with negative sign is a difference from the density contribution. Due to this extra, the chiral restoration by rotation is weaker than that by density. Therefore the suppression of
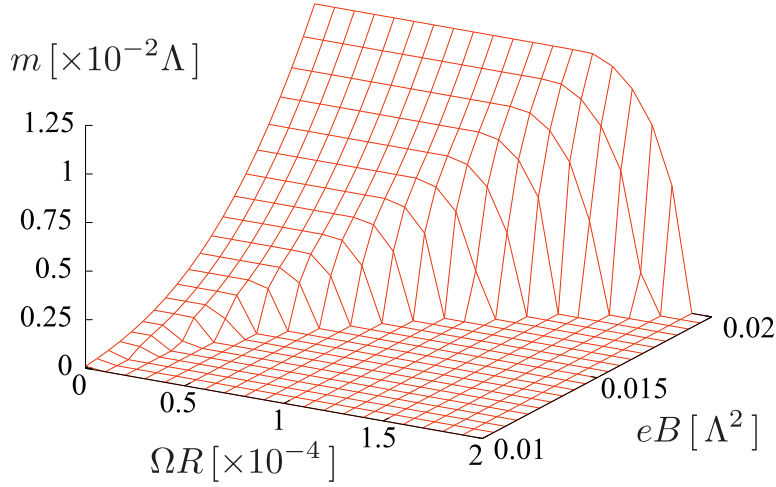
Figure 4.6: Dynamical mass as a function of Ω and eB at weak coupling [76]. For small Ω the dynamical mass is exponentially enhanced with $1/eB$ (i.e. the magnetic catalysis).

the dynamical mass in the rotating system (the red line in Fig. 4.5) is more gradually than that in the finite-density system (the blue line in Fig. 4.5). Additionally, from Eq. (4.35) we find $F_\Omega < F_\mu$ for a fixed μ_N. Thus the chiral restoration by rotation need larger μ_N than that by finite density, as shown in Fig. 4.5.

(II) Critical value of angular velocity

From Eq. (4.35), we can analytically obtain the critical angular velocity above which the dynamical mass vanishes. Since the dynamical mass generation stems from the physics of the infrared modes, the regularization scheme should be irrelevant. If we utilized the proper time regularization [107], we would obtain the following gap equation, instead of Eq. (4.25):

$$
\begin{aligned}
\frac{4\pi^2}{G} =& \Lambda_{\mathrm{PT}}^2 - m^2 \left[\ln\left(\frac{\Lambda_{\mathrm{PT}}^2}{2eB} \right) - \gamma_{\mathrm{EM}} \right] \\
&+ eB \left[\ln\left(\frac{m^2}{4\pi eB} \right) + 2\ln\Gamma\left(\frac{m^2}{2eB} \right) - 2\ln\left(\frac{\mu_N + \sqrt{\mu_N^2 - m^2}}{m} \right) + 2\sqrt{1 - \frac{m^2}{\mu_N^2}} \right],
\end{aligned}
\tag{4.36}
$$

where γ_{EM} is the Euler-Mascheroni constant, $\Gamma(z)$ denotes the gamma function, and Λ_{PT} stands for the cutoff parameter in the proper-time regularization. The last two terms in the second line result from the contribution of the $n = 0$ mode in Eq. (4.35). From the above gap equation in the limit of $m \to 0$, we analytically obtain the following critical Ω:

$$
\Omega_c(eB) = \frac{\sqrt{\pi}}{S\sqrt{eB}} \exp\left[-\frac{2\pi^2}{eB}\left(\frac{1}{G} - \frac{1}{G_c} \right) + 1 \right] \simeq \frac{1.53 \times 10^{-6}}{\sqrt{eB}} \exp\left(-\frac{0.610\Lambda^2}{eB} \right),
\tag{4.37}
$$

where $G_c = 4\pi/\Lambda_{\mathrm{PT}}^2$ is the critical coupling calculated without rotation and magnetic field. The last expression in Eq. (4.37) is obtained with substituting the parameters in Table 4.1. On the
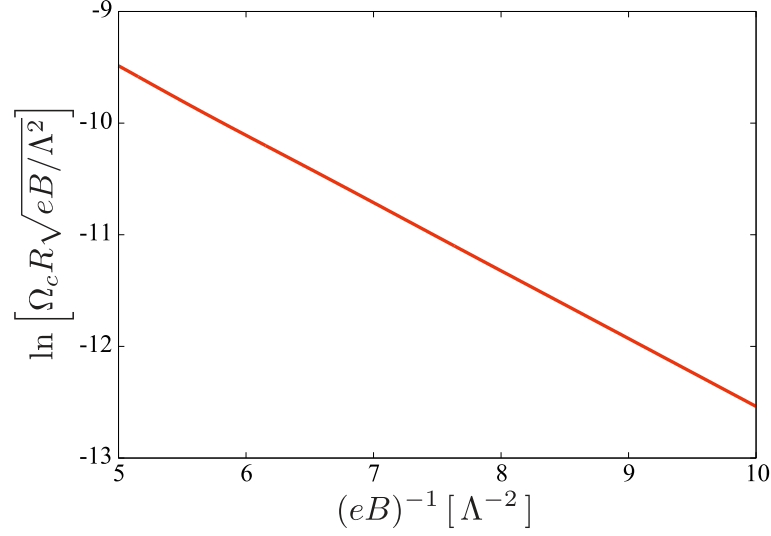
Figure 4.7: eB-dependence of Ω_c for $0.1\,\Lambda^2 \leq eB \leq 0.2\,\Lambda^2$ [76].

other hand, from the eB-dependence of Ω_c shown in Fig. 4.7, we perform numerically evaluate the critical value as

$$\Omega_c(eB) \simeq \frac{1.58 \times 10^{-6}}{\sqrt{eB}} \exp\left(-\frac{0.609\Lambda^2}{eB}\right). \tag{4.38}$$

This fitting result ensures that the integral representation (4.34) is a good approximation for the parameters in Table 4.1.

4.5 Dynamical mass for strong coupling

Let us see the strong coupling case. In Figure 4.8 we show the numerical results. Here are discussions about the numerical results.

(I) Magnetic suppression of the dynamical mass in rotating systems

It is obvious that the magnetic response in Fig. 4.8 is different from that in Fig. 4.6. For small angular velocity, the dynamical mass is almost independent of Ω and eB. For large Ω, the dynamical mass is suppressed as magnetic field increases. This is thus a counterpart of the finite-density inverse magnetic catalysis. We name such a magnetic suppression of the dynamical mass the "rotational magnetic inhibition" [76]. We find also that the damping starts at $\mu_N = \Omega N \sim \sqrt{eB}$. This is similar to the finite-density inverse magnetic catalysis, which is observed at $\mu \sim \sqrt{eB}$ [41].

We note that such a drastic difference between Figs. 4.6 and 4.8 originates in the contribution of higher Landau levels to the dynamics. In the weak coupling case only a few lower Landau levels is relevant to the gap equation. On the other hand many more Landau levels get involved
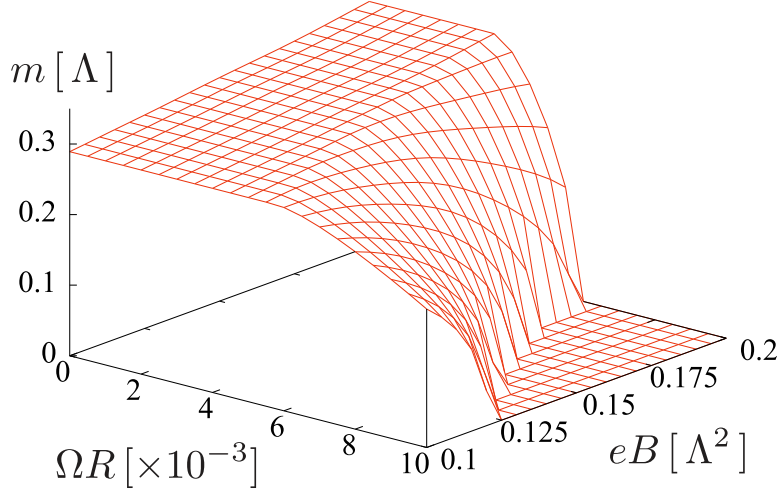
Figure 4.8: Dynamical mass as a function of Ω and eB at strong coupling [76]. At large Ω, chiral symmetry is restored by eB, which is the rotational magnetic inhibition.

for the strong coupling. This is essential for the realization of the rotational magnetic inhibition, as well as of the inverse magnetic catalysis at finite density.

(II) de Haas-van Alphen oscillation

We compare more precisely the finite-density inverse magnetic catalysis and the rotational magnetic inhibition. It is known that for strong coupling $G > G_c$, the interplay between μ and eB generates many local minima in the QCD vacuum [31], due to the de Haas-van Alphen oscillation [103, 104]. In other words, the dynamical mass becomes an oscillational function of μ^2/eB. In contrast, the mass in Fig. 4.8 does not show such a structure. To clarify the reason of this, we first review the original argument of the de Haas-van Alphen oscillation. Let us investigate the profile of the following function:

$$F(m) = \frac{1}{G} - \frac{1}{\pi}(F_0 - F_\mu) \,, \tag{4.39}$$

whose zero corresponds to the nontrivial solution in Eq. (4.29). This function itself is continuous for any m, but its derivative is not:

$$\frac{dF_0(m)}{dm} = -\frac{meB}{2\pi} \sum_{n=0}^{\infty} \alpha_n \int_0^\infty \frac{dp_z \, f(p; \Lambda, \delta\Lambda)}{(p_z^2 + \varepsilon_{\text{tr}}^2)^{3/2}} \,, \tag{4.40}$$

$$\frac{dF_\mu(m)}{dm} = \frac{meB}{2\pi} \sum_{n=0}^{\infty} \alpha_n \left[\int_0^{q_{\ell,n}} \frac{dp_z \, \theta(|\mu| - \varepsilon_{\text{tr}})}{(p_z^2 + \varepsilon_{\text{tr}}^2)^{3/2}} + \frac{\theta(|\mu| - \varepsilon_{\text{tr}})}{|\mu|\sqrt{\mu^2 - \varepsilon_{\text{tr}}^2}} \right] \tag{4.41}$$

The second term in Eq. (4.41) positively diverges at

$$m = \sigma_n \equiv \sqrt{\mu^2 - 2neB} \,. \tag{4.42}$$

and Eq. (4.41) becomes zero if m is slightly larger than σ_n. Namely we find

$$\left.\frac{dF(m)}{dm}\right|_{m \to \sigma_n - 0} = -\infty \,, \qquad \left.\frac{dF(m)}{dm}\right|_{m \to \sigma_n + 0} > 0 \,, \tag{4.43}$$

which shows the nonmonotonicity of $F(m)$. This behavior in the vicinity of $m = \sigma_n$ is the direct origin of the de Haas-van Alphen oscillation for the dynamical mass [31].

On the other hand, at least in rotating systems with our parameter choice, such an oscillating profile does not appears. Since in the case with rotation, we replace F_μ with F_Ω defined in Eq. (4.27), the singular part of $dF(m)/dm$ is obtained as

$$\begin{aligned}
&\frac{meB}{2\pi} \sum_{n=0}^{\infty} \alpha_n \frac{\theta(|\mu| - \varepsilon_{\text{tr}})}{|\mu|\sqrt{\mu^2 - \varepsilon_{\text{tr}}^2}} \\
&\longrightarrow \frac{m}{S} \sum_{n=0}^{\infty} \alpha_n \sum_{\ell=-n}^{N-n} \frac{\theta(\Omega|\ell + 1/2| - \varepsilon_{\text{tr}})}{\Omega|\ell + 1/2|\sqrt{\Omega^2(\ell + 1/2)^2 - \varepsilon_{\text{tr}}^2}} f(\Omega|\ell + 1/2|; \Lambda, \delta\Lambda),
\end{aligned} \tag{4.44}$$

where the cutoff function is additionally involved, similarly to that in Eq. (4.27). However for $\mu_N = \Omega N \lesssim \Lambda$, we can practically remove the cutoff function from the third term in Eq. (4.44). Then the ℓ-sum is approximately written by an integration, as well as in Eq. (4.34):

$$\begin{aligned}
\sum_{\ell=-n}^{N-n} \frac{\theta(\Omega|\ell + 1/2| - \varepsilon_{\text{tr}})}{\Omega|\ell + 1/2|\sqrt{\Omega^2(\ell + 1/2)^2 - \varepsilon_{\text{tr}}^2}} &\simeq \frac{1}{\Omega} \int_{\varepsilon_{\text{tr}}}^{\mu_N} \frac{d\mu\, \theta(\mu_N - \varepsilon_{\text{tr}})}{\mu\sqrt{\mu^2 - \varepsilon_{\text{tr}}^2}} \\
&= \frac{1}{\Omega\varepsilon_{\text{tr}}} \left[\frac{\pi}{2} - \tan^{-1}\left(\frac{\varepsilon_{\text{tr}}}{\sqrt{\mu_N^2 - \varepsilon_{\text{tr}}^2}}\right)\right] \theta(\mu_N - \varepsilon_{\text{tr}}) \,,
\end{aligned} \tag{4.45}$$

which is finite even at $m = \sqrt{\mu_N^2 - 2neB}$. For $\mu_N > \Lambda$, taking the replacement $\mu_N \to \Lambda$, we can similarly confirm the absence of the singularity in Eq. (4.44). Hence $F(m)$ in our analysis can be regarded as a monotonic function, which does not lead to the de Haas-van Alphen oscillation in Fig. 4.8.

(III) Rotational magnetic inhibition in realistic systems

Our result for the rotational magnetic inhibition could be applied to realistic systems. First let us estimate the necessary angular velocity in a condensed matter system involving pseudo-relativistic fermionic modes, such as graphene or 3D Dirac semimetals. We consider the system with the radius $R = 10\,\text{cm}$ in the magnetic field $B = 1.7 \times 10^4\,\text{G}$. Since the rotational magnetic inhibition becomes visible at $\mu_N = \Omega N \sim \sqrt{eB}$ (see Fig. 4.8), we find that the rotational magnetic inhibition is observed at $\Omega \sim \sqrt{eB}v_F/N \simeq 2.5 \times 10^3\,\text{s}^{-1}$, which is an experimentally possible value [109]. Here we employ $v_F = 10^6\,\text{m/s}$, which is a typical value of the Fermi velocity in graphene [110]. Therefore in a table-top experiment, we should confirm the realization of the rotational magnetic inhibition.

A more interesting environment is neutron stars. For a millisecond pulsar with $\Omega \sim 10^3\,\text{s}^{-1}$ and $R \sim 10^4\,\text{m}$, the velocity on the edge of star reads $\Omega R \sim \mathcal{O}(10^{-1})$. The numerical result in

Fig. 4.8 suggests that chiral symmetry should be restored at small eB. In other words, this novel phenomenon could affect the equation of state (EoS) for neutron stars; the rotational magnetic inhibition stiffens the neutron star EoS through the chiral symmetry restoration. Actually to obtain the quantitative suggestion, it is necessary to analyze the chiral symmetry breaking in a system with $R \simeq 10^4$ m, which is larger than the radius we chose in the current study. Although such a evaluation could be our future task, we emphasize that the chiral condensate in larger rotating system is more sensitive to rotation because the effective chemical potential μ_N is proportional to R^2. Thus, the rotational magnetic inhibition should be a significant effect for the neutron star physics.

Chapter 5

Summary

In Chapter 2, we gave a brief review of the quantum physics in rotating systems. Rotation has two aspects analogous to environmental sources: magnetic field and density. The former is reflected in the mathematical correspondence between the Lorentz force and the Coriolis force. As a result, rotation leads to several magnetic-like phenomena, such as the vortex of the Bose-Einstein condensate, the quantum Hall effect, and the chiral vortical effect. In the realization of them, we need to cancel out the centrifugal force with a trapping potential, or to take the approximation to neglect higher order terms of angular velocity (or vorticity). This means that in relativistic field theory, rotation with large angular velocity cannot solely create the magnetic environment.

We can also regard rotating systems as a fictitious finite-density system. This is a more ubiquitous analogy that does not require any extra source or any approximation, unlike that to magnetism. The analogy between density and rotation is readily understood if it is noticed that the rotational energy shift plays the role of an effective chemical potential. Namely we expect that the thermodynamics in rotating systems is easily formulated in the same way to the density case. For rotating bosons, however, we immediately conflict a pathological problem: for large angular velocity, the distribution function seems negative, and so ill-defined. Such an unexpected situation emerges as long as rotation is treated in relativity. In other word, to keep the relativistic causality in terms of rotation, we should properly take into account the boundary effect. Indeed we explicitly confirmed that the Dirichlet boundary condition for a rotating cylinder leads to the well-defined Bose-Einstein distribution function. At the same time, this means that the vacuum in the rotating frames is the same as in the Minkowski spacetime, and thus rotation does not affect the bosonic thermodynamics at zero temperature.

In Chapter 3, we constructed the fundamental framework for the analysis of rotating fermionic matter, including the chiral symmetry breaking in the presence of rotation. Based on the argument of the quantum field theory in curved spacetime, we solved the Dirac equation for free fermions in a finite-size rotating cylinder. As well as rotating scalars, a proper treatment of the boundary is necessary to investigate rotating fermionic matter, but the Dirichlet-type condition is not applicable to fermions. Instead, imposing the boundary condition in terms of

the fermionic flux, we obtained the energy spectrum with an infrared energy gap. By using the solutions for the Dirac equation, we analyzed the NJL model in rotating systems at zero temperature. From the resulting NJL gap equation, we analytically found that the finite infrared energy gap prohibits rotation affecting thermodynamic at zero temperature. Therefore rotation cannot affect thermodynamic at zero temperature. This would be understood as a similar situation to the finite-density system with a chemical potential less than mass threshold. In other words, we showed that the boundary of systems should plays the most important role for rotating matter. If the thermodynamic limit is taken in rotating systems, we could arrived at the incorrect result that rotation solely induces a phase transition [77]. This suggestion should be the basis of QCD with rotation, which is applied to the future investigation of relativistic rotating systems, such as non-central heavy-ion collisions and compact stars. Also we numerically computed the spatial profile of the dynamical mass in the cylinder at zero temperature. From this result, we confirmed the validity of the local density approximation to numerically evaluate the inhomogeneous dynamical mass.

Although the rotational effect is invisible at zero temperature, we can see it in the case that the boundary effect can be neglected somehow. The first case is a high-temperature system because the thermal screening permits us to neglect the boundary effect. Indeed from the numerical calculation, we confirmed that rotation induces the chiral restoration at finite temperature. This is consistent with the argument that an axial current is induced by rotation at high temperature in Ref. [81–83]. This current are related to quantum anomaly, as suggested by the analysis with the gauge-gravity duality. The topological structure is however unclear in the original derivation within the Dirac field theory in rotating systems. From the viewpoint of the recent study of the transport phenomena in a quark-gluon plasm, we should need more deep understanding for anomalous aspects of rotating matter.

The second case is a strongly magnetized system. In a strong magnetic field, wave functions are tightly localized, and thus the particles cannot feel the existence of the boundary. We also mentioned that even at zero chemical potential, rotation leads to a finite number density, which is provided by the interplay between magnetic field and rotation. This is an actual manifestation of the analogy between density and rotation. Interestingly, we found that the number density induced by rotation contains an anomalous contribution. Thus the dynamics of rotating matter is fundamentally connected to quantum anomaly, which comes out through combining with temperature or magnetic field.

In Chapter 4, we first reviewed the basic idea of the magnetic response of chiral condensate. Both in the magnetic catalysis and the inverse magnetic catalysis, the crucial concept is that through the Landau quantization, the density of states for the infrared mode (i.e. the lowest Landau level) becomes large. Therefore, the chiral structure is expected to be unchanged even with rotation as long as energy levels are Landau-quantized.

Next we analyzed the Dirac equation both with magnetic field and rotation. Due to the localization of the wave functions, the boundary effect is irrelevant to dynamics in a strong

magnetic field. For this reason, we solved the Dirac equation without considering the boundary condition, and showed that rotation modify the Landau levels and resolve the Landau degeneracy. We also investigated the chiral structure in a rotating magnetized system. In the weak coupling case (where chiral symmetry is not yet broken in the vacuum), the dynamical mass is generated and enhanced by the magnetic field, which is nothing but the magnetic catalysis. Together with rotation, we found that the dynamical mass is suppressed with increasing angular velocity. In the strong coupling case (where chiral symmetry breaking is already broken in the vacuum), we discovered the opposite magnetic response of the dynamical mass; at a finite angular velocity, the dynamical mass decreases with increasing magnetic field. Such a chiral restoration induced by magnetic field is an inverse phenomenon of the conventional magnetic catalysis. As an analogous phenomenon to the inverse magnetic catalysis at finite density, we named this novel phenomenon the "rotational magnetic inhibition."

We also suggested possible applications of the rotational magnetic inhibition. We could discuss the realization of this phenomenon, e.g. in condensed matter systems, in the cores of the neutron star, and in noncentral relativistic heavy-ion collision experiments [111]. For the heavy-ion collision the estimate of Ω is still unclear, and it is difficult to make any decisive statement (although the vorticity could be computed [54]). For a condensed matter system, we confirmed from a brief estimate that the rotational magnetic inhibition should be observed in a table-top experiment. For the neutron star, angular velocity itself is much smaller than the QCD scale. However rotation contributes to the dynamics through the combination with angular momentum, namely the rotational energy shift or the effective chemical potential. For this reason, our results showed that the rotation should give a sizable modification to the dynamical mass through an effective chemical potential $\mu_N = \Omega N \propto R^2$. This suggested that we should consider the rotational effect on the neutron star EoS; its angular velocity has seemed too small to affect the QCD dynamics, and only a global effect of rotaiton has been considered in the construction EoS [112] (see also Refs. [113–116]).

Our framework constructed in this thesis is obviously applicable to the system with other environmental parameters. For instance, since finite chemical potential shifts the Fermi surface, the rotational effect should be visible in the real finite-density system, even at zero temperature. For the neutron star physics, it is most necessary to investigate rotating matter with finite chemical potential. In this case, it is expected that the necessary angular velocity for the rotational magnetic inhibition decreases due to the support of the real chemical potential.

In rotating systems, it is important to analyze spatial inhomogeneity [90]. Intuitively the chiral condensate could decrease as r (the radial distance from the rotational axis) increases because the geometry in rotating frames is more deformed with larger r. Nevertheless for the analysis for magnetized rotating matter in Chapter 4, we assumed a homogeneous condensate. For this reason we obtained our numerical results dependent on the system size R, not on the local coordinate r. Such an assumption is useful for the manifestation of the analogy between rotation and density, but including this spatial inhomogeneity should be necessary for more

precise discussion.

Finally we comment about the realistic rotating systems. In this thesis, we treat the rotational effect as follows. In a rotating container with angular velocity Ω, the confined classical viscous fluid also rotates with the same Ω since the fluid interacts with the microscopically rough wall (boundary) of the container. In this case, through the coordinate transformation to the rotating frame, the rotational effect could be taken into account as the rotational energy shift, which plays the role of an effective chemical potential. This is the basis of the discussion for a rotating Bose-Einstein condensate. Also for rigidly rotating systems, e.g. compact stars, the argument with homogeneous rotation should be usable (although it is necessary to consider a spherical rotating frame with gravity).

On the other hand, for fluid with small viscosity, each particle in the rotating container cannot possess the same angular velocity immediately. From the viewpoint of the field theory, such a fluid corresponds to strongly interacting systems, where the mean free pass is short. Thus the above brief argument might be not simply applicable to quark-gluon plasma, which can be regarded as a perfect fluid with much small viscosity [117]. In other words, if the relaxation time after externally driving rotation is short enough compared with the typical time scale, then the picture as the rigid-body rotation is much reliable. Contrary if not, the hydrodynamic description should be utilized instead of the field theory in rotating frames. For example, in Refs. [118–122], the hydrodynamics has been employed to describe the thermodynamics in rotating systems through the Poincaré algebra. (We note that the chiral symmetry breaking has not been discussed there.) Furthermore not only more quantitative discussion with phenomenological analysis but also the experimental estimation of the angular momentum of hot matter in heavy-ion collisions should be required to clarify the rotational effect on QCD.

Acknowledgements

Appendix A

Dirac equation in a rotating frame

A.1   Solution without magnetic field

We solve the Dirac equation in the presence of rotation. From Eq. (3.6) we obtain the equation in the cylindrical coordinate:

$$
\begin{aligned}
0 &= [i\gamma^\mu(\partial_\mu + \Gamma_\mu) + m][i\gamma^\mu(\partial_\mu + \Gamma_\mu) - m]\psi \\
&= \left[\left(i\partial_0 - i\Omega\partial_\theta + \Omega\frac{\sigma^{12}}{2} \right)^2 + \partial_r^2 + \frac{1}{r}\partial_r + \frac{1}{r^2}\partial_\theta^2 + \partial_3^2 - m^2 \right]\psi .
\end{aligned}
\tag{A.1}
$$

A positive energy solution for this equation can be represented as

$$
\psi = u_\pm = e^{-iEt + ip_z z} \begin{pmatrix} \eta_\pm \\ \lambda_\pm \end{pmatrix} .
\tag{A.2}
$$

where

$$
\eta_\pm(r,\theta) = e^{i\ell_\pm\theta}\tilde{\eta}_\pm(r)\chi_\pm , \quad \sigma^3\chi_\pm = \pm\chi_\pm ,
\tag{A.3}
$$

and $\lambda_\pm$ is obtained from $\eta_\pm$. Because of the rotational invariance in Eq. (A.1), the solution η should be the eigenfunction of the total angular momentum $\hat{J}_z = \hat{L}_z + \sigma^3/2$. This means that

$$
\ell_+ + 1/2 = \ell_- - 1/2 , \quad \text{i.e.} \quad \ell_+ = \ell_- - 1 \equiv \ell .
\tag{A.4}
$$

With such an ansatz, Eq. (A.1) is reduced to the equation for the scalar function $\varphi_\pm$:

$$
\left[\partial_r^2 + \frac{1}{r}\partial_r - \frac{\ell_\pm^2}{r^2} - p_{\ell,k}^2 \right] \tilde{\eta}_\pm = 0 ,
\tag{A.5}
$$

where the transverse momentum is defined as $p_{\ell,k}^2 = \left[E + \Omega(\ell + 1/2) \right]^2 - p_z^2 - m^2$. For this differential equation, the nonsingular solution at $r = 0$ is given by the Bessel function of the first kind, i.e. $\tilde{\eta}_\pm(r) = J_{\ell_\pm}(p_\perp r)$, and thus we arrive at

$$
\begin{aligned}
\tilde{\eta}_+(r,\theta) &= e^{i\ell\theta}J_\ell(p_{\ell,k}r)\chi_+ \equiv \phi_{\ell,k}(r,\theta)\chi_+ , \\
\tilde{\eta}_-(r,\theta) &= e^{i(\ell+1)\theta}J_{\ell+1}(p_{\ell,k}r)\chi_- \equiv \varphi_{\ell,k}(r,\theta)\chi_- .
\end{aligned}
\tag{A.6}
$$

Now λ is determined from Eq. (3.6) with the above η. In the Dirac representation, $u_\pm$ takes the following form:

$$u_\pm = \frac{e^{-iEt+ip_z z}}{\sqrt{\varepsilon + m}} \begin{pmatrix} (\varepsilon + m)\eta_\pm \\ -i\sigma^i \partial_i \eta_\pm \end{pmatrix} = \frac{e^{-iEt+ip_z z}}{\sqrt{\varepsilon + m}} \begin{pmatrix} (\varepsilon + m)\eta_\pm \\ (\sigma^+ \hat{p}_+ + \sigma^- \hat{p}_- + \sigma^3 \hat{p}_z)\eta_\pm \end{pmatrix} \tag{A.7}$$

with $\varepsilon = |E + \Omega(\ell + 1/2)|$, $\sigma^\pm = \sigma^1 \pm \sigma^2$, and $\hat{p}_\pm = -i(\partial_1 \pm \partial_2)$. We note that $\hat{p}_\pm$ play the role of the ladder operators with respect to ℓ. Indeed using the recursion relation of the Bessel function

$$\left[\pm \partial_x + x^{-1}(\ell \pm 1) \right] J_{\ell \pm 1}(x) = J_\ell(x) , \tag{A.8}$$

we find that the scalar functions $\phi_{\ell,k}$ and $\varphi_{\ell,k}$ are interchanged each other:

$$\begin{aligned} \hat{p}_+ \phi_{\ell,k} &= -ie^{i\theta}(\partial_r + ir^{-1}\partial_\theta)\phi_{\ell,k} = ip_{\ell,k}\varphi_{\ell,k} , \\ \hat{p}_- \varphi_{\ell,k} &= -ie^{-i\theta}(\partial_r - ir^{-1}\partial_\theta)\varphi_{\ell,k} = -ip_{\ell,k}\phi_{\ell,k} . \end{aligned} \tag{A.9}$$

Finally we obtain the positive energy solution (3.8):

$$u_+ = \frac{e^{-iEt+ip_z z}}{\sqrt{\varepsilon + m}} \begin{pmatrix} (\varepsilon + m)\phi_{\ell,k} \\ 0 \\ p_z \phi_{\ell,k} \\ ip_{\ell,k} \varphi_{\ell,k} \end{pmatrix} , \quad u_- = \frac{e^{-iEt+ip_z z}}{\sqrt{\varepsilon + m}} \begin{pmatrix} 0 \\ (\varepsilon + m)\varphi_{\ell,k} \\ -ip_{\ell,k} \phi_{\ell,k} \\ -p_z \varphi_{\ell,k} \end{pmatrix} . \tag{A.10}$$

From $v_\pm = i\gamma^2 u_\pm^*$ we also obtain the negative energy solution (3.10).

A.2 Solution with a magnetic field

We solve the Dirac equation in the presence of rotation and magnetic field. Then we show that the solution is the Landau wave function, and that the quantum number ℓ is the same as without rotation.

First the Dirac equation (4.9) leads to the following equation:

$$\begin{aligned} 0 &= [i\gamma^\mu(D_\mu + \Gamma_\mu) + m][i\gamma^\mu(D_\mu + \Gamma_\mu) - m]\psi \\ &= \left[\left(i\partial_0 - i\Omega\partial_\theta + \Omega\frac{\sigma^{12}}{2} \right)^2 + \partial_r^2 + \frac{1}{r}\partial_r + \frac{1}{r^2}\partial_\theta^2 \right. \\ &\qquad \left. + eB(-i\partial_\theta + \sigma^{12}) - \left(\frac{eBr}{2} \right)^2 + \partial_3^2 - m^2 \right] \psi . \end{aligned} \tag{A.11}$$

The last line is written with the cylindrical coordinate $x^\mu = (t, r, \theta, z)$. As well as without magnetic field, we have an ansatz of the positive energy solution for this equation:

$$\psi = u_\pm = e^{-iEt+ip_z z} \begin{pmatrix} \eta_\pm \\ \lambda_\pm \end{pmatrix} , \tag{A.12}$$

with

$$\eta_\pm(r,\theta) = e^{i\ell_\pm\theta}\tilde{\eta}_\pm(r)\chi_\pm \ , \tag{A.13}$$

where $\ell_\pm$ is an integer and $\chi_\pm$ is the spin eigenstate; $\sigma^3\chi_\pm = \pm\chi_\pm$. The rotational invariance imposes the condition between ℓ_+ and ℓ_-, i.e. Eq. (A.4). We note that Eq. (A.4) is the only constraint for ℓ at this stage. From this ansatz, we find that $\tilde{\eta}_\pm$ is the determined by the following equation:

$$\left[\left\{E + \Omega(\ell_\pm \pm 1/2)\right\}^2 + \partial_r^2 + \frac{1}{r}\partial_r - \frac{\ell_\pm^2}{r^2}\right.$$
$$\left. + eB(\ell_\pm \pm 1) - (eBr/2)^2 - p_z^2 - m^2\right]\tilde{\eta}_\pm = 0 \ . \tag{A.14}$$

The general solution for this equation is given by the following form with the confluent hypergeometric functions:

$$\tilde{\eta}_\pm = r^{|\ell_\pm|}e^{-eBr^2/4}\left[c_1 M(a, |\ell_\pm| + 1, eBr^2/2)\right.$$
$$\left. + c_2(eBr^2/2)^{-|\ell_\pm|}M(a - |\ell_\pm|, 1 - |\ell_\pm|, eBr^2/2)\right] \ , \tag{A.15}$$

where c_1 and c_2 denote integral constants, and a is defined as

$$a = \frac{1}{2eB}\left[eB\left(|\ell_\pm| \mp 1 - \ell_\pm + 1\right) - \left\{E + \Omega(\ell_\pm \pm 1/2)\right\}^2 + p_z^2 + m^2\right] \ . \tag{A.16}$$

Let us identify the solution that respects boundary conditions. Here $\tilde{\eta}_\pm$ should be normalizable, and so be finite at arbitrary r. The finiteness of $\tilde{\eta}_\pm(r \to 0)$ requires $c_2 = 0$. Besides $\tilde{\eta}_\pm(r \to \infty)$ has no singularity only if a is a nonpositive integer:

$$n_p \equiv -a = 0, 1, 2, \cdots \ . \tag{A.17}$$

In this case, this hypergeometric function is reduced to an associated Laguerre polynomial:

$$M(-n_p, |\ell_\pm| + 1, eBr^2/2) \propto L_{n_p}^{|\ell_\pm|}(eBr^2/2) \ . \tag{A.18}$$

From Eq. (A.17), we find that the energy dispersion relation is quantized:

$$\left[E + \Omega(\ell_\pm \pm 1/2)\right]^2 = eB(2n_p + |\ell_\pm| - \ell_\pm + 1 \mp 1) + p_z^2 + m^2 \ . \tag{A.19}$$

This dispersion can be reduced to Eq. (4.10) if we introduce the new integers defined by

$$n = n_+ = n_- + 1,$$
$$n_\pm \equiv n_p + \frac{1}{2}\left(|\ell_\pm| - \ell_\pm + 1 \mp 1\right) \ . \tag{A.20}$$

We note that these equations imply the lower bounds for $\ell_\pm$:

$$\ell = \ell_+ = \ell_- - 1 \geq -n . \tag{A.21}$$

Finally using the property of the Laguerre function,

$$L_{n+\ell}^{-\ell}(x^2) \propto x^{2\ell} L_n^\ell(x^2) \quad (\text{for } \ell \leq 0) , \tag{A.22}$$

we obtain the eigenfunction as the following simpler form:

$$\tilde{\eta}_{n,\ell}(r) \propto r^\ell e^{-eBr^2/4} L_n^\ell(eBr^2/2) . \tag{A.23}$$

We mention that the solution is derived similarly even for $\Omega = 0$, and so the quantum number ℓ is the same as without rotation. Therefore the possible range of ℓ in a rotating frame is also defined by Eq. (4.14) (see in the discussion in Appendix B).

We here emphasize that the essential requirement for the Landau quantization is the boundary condition at $r \to \infty$; the wave function should converge at infinity. Therefore the energy dispersion for charged particles is Landau-quantized only if the size of system is infinite. In other words for the Landau quantization in the cylindrical system, its radius is large enough compared with the magnetic length, i.e. $R \gg l_B = 1/\sqrt{eB}$, as discussed in Section 4.2. In the system with a size comparable to or smaller than ℓ_B, we should properly take into account the boundary condition, as well as in Chapter 3. In such a case, n_p is differently quantized from Eq. (A.17).

Appendix B

Landau degeneracy in cylinders

Based on the Klein−Gordon equation for charged scalars in external magnetic field, we briefly show that the Landau degeneracy factor in the cylindrical coordinate is the same as in Cartesian coordinate. As a result we find that the range of the quantum number ℓ for the nth Landau level is given by Eq. (4.14).

B.1   Landau quantization for general gauges

For general gauge we prepare the Landau quantization. In a magnetic field $\boldsymbol{B} = B\hat{z}$ (i.e. $B^i = \epsilon_{ijk}\partial^j A^k$) the Klein–Gordon equation for charged scalar particles reads

$$\left(\partial_0^2 - \partial_3^2 + m^2 - D_1^2 - D_2^2\right)\Phi = 0 \tag{B.1}$$

with $D_i = \partial_i + ieA_i$. Since the solution is given by $\Phi = e^{-i\varepsilon t + ip_z z}\phi(x, y)$, this equation is then reduced to

$$\hat{H}\phi = \lambda\phi \tag{B.2}$$

with $\hat{H} = -(D_1^2 + D_2^2)$ and $\lambda = \varepsilon^2 - p_z^2 - m^2$. Under the gauge condition $B^i = \epsilon_{ijk}\partial^j A^k$, the operator $\hat{H}$ can be written with

$$\hat{H} = eB(2a^\dagger a + 1) \,, \tag{B.3}$$

where we define the ladder operators

$$a \equiv \frac{i}{\sqrt{2eB}}(D_1 + iD_2) \,, \quad a^\dagger \equiv \frac{i}{\sqrt{2eB}}(D_1 - iD_2) \,, \tag{B.4}$$

which satisfy $[a, a^\dagger] = 1$. Namely the eigenstates for Eq. (B.2) are $|n\rangle \propto (a^\dagger)^n|0\rangle$, and the corresponding eigenvalue is obtained as the Landau energy levels; $\lambda = eB(2n + 1)$. Therefore the energy dispersion is given by

$$\varepsilon = \pm\sqrt{eB(2n + 1) + p_z^2 + m^2} \,. \tag{B.5}$$

B.2   Landau quantization for symmetric gauge

When we utilize the cylindrical coordinate, the symmetric gauge $A_\mu = (0, By/2, -Bx/2, 0)$ is most useful because the Hamiltonian in Eq. (B.2) respects the rotational symmetry. Instead of (r, θ), we use the complex coordinate defined by

$$z \equiv x + iy , \quad \bar{z} \equiv x - iy . \tag{B.6}$$

and we introduce the new notations for the derivatives $\partial \equiv \partial/\partial z$ and $\bar{\partial} \equiv \partial/\partial \bar{z}$. Then the ladder operators are also rewritten with them:

$$a = \frac{-i}{\sqrt{2eB}} \left(2\bar{\partial} + \frac{eB}{2} z \right) , \quad a^\dagger = \frac{-i}{\sqrt{2eB}} \left(2\partial - \frac{eB}{2} \bar{z} \right) . \tag{B.7}$$

The ground state is defined with the condition $a|0\rangle = 0$:

$$\langle z, \bar{z}|a|0\rangle = -i\frac{1}{\sqrt{2eB}} \left(2\bar{\partial} + \frac{eB}{2} z \right) \phi(z, \bar{z}) = 0 . \tag{B.8}$$

The solution is given by

$$\phi(z, \bar{z}) = \tilde{\phi}(z)e^{-eBz\bar{z}/4} , \tag{B.9}$$

where $\tilde{\phi}(z)$ denotes a function of z. In principle, we have no condition for the choice of $\tilde{\phi}(z)$, except for the analyticity. Such an ambiguity of $\tilde{\phi}(z)$ comes from assuming an infinitely large system in our calculation. In other words, the eigenvalue equation of the harmonic oscillator cannot be solved in finite-size systems (see Appendix A.2).

In order to find $\tilde{\phi}(z)$, we analyze another quantum number, i.e. the canonical angular momentum. Because of the rotational invariance of the Hamiltonian, the corresponding eigenstate can be also the eigenstate of the angular momentum $\hat{L}_z = xp_y - yp_x = z\partial - \bar{z}\bar{\partial}$. Let us introduce the new ladder operators:

$$b \equiv \frac{1}{\sqrt{2eB}} \left(2\partial + \frac{eB}{2} \bar{z} \right), \quad b^\dagger \equiv \frac{1}{\sqrt{2eB}} \left(-2\bar{\partial} + \frac{eB}{2} z \right) , \tag{B.10}$$

which satisfy $[b, b^\dagger] = 1$. We represent the angular momentum as the ladder operators:

$$\hat{L}_z = b^\dagger b - a^\dagger a . \tag{B.11}$$

We define the simultaneous eigenstates for $a^\dagger a$ and $b^\dagger b$:

$$a^\dagger a|n, n_p\rangle = n|n, n_p\rangle, \quad b^\dagger b|n, n_p\rangle = n_p|n, n_p\rangle , \tag{B.12}$$

for $n, n_p = 0, 1, \cdots$. Instead of n_p, we designate these eigenstates by the new quantum number $\ell = n_p - n$:

$$\begin{aligned}
\langle z, \bar{z}|n, n_p\rangle &= \phi_{nn_p}(z, \bar{z}) \equiv \psi_{n\ell}(z, \bar{z}) , \\
\hat{L}_z \psi_{n\ell} &= (b^\dagger b - a^\dagger a)\psi_{n\ell} = \ell\psi_{n\ell} .
\end{aligned} \tag{B.13}$$

We note that the non-negativities of n and n_p lead to the lower bound of ℓ:

$$\ell \geq -n \ . \tag{B.14}$$

We produce a ground state by the operation of ladder operator $b^\dagger$:

$$\begin{aligned}
\psi_{0\ell}(z, \bar{z}) &\propto (b^\dagger)^\ell \psi_{00}(z, \bar{z}) \\
&\propto z^\ell e^{-eBz\bar{z}/4} \ .
\end{aligned} \tag{B.15}$$

From this eigenstate, we find that ℓ corresponds to the degenerate quantum number, which is irrelevant to the energy level. Thus the possible range of ℓ is nothing but the Landau degeneracy factor. In order to calculate the degeneracy factor, we focus on the following equation:

$$\frac{d}{dr}(2\pi r |\psi_{0\ell}|^2) = 0 \ , \tag{B.16}$$

which determines the radius that gives the maximum value of this distribution. If we consider the system to be the cylinder with radius R, the solution for Eq. (B.16) should be smaller than R, which leads to the upper bound of ℓ:

$$\ell \leq \frac{eBR^2}{2} = \frac{eBS}{2\pi} \ . \tag{B.17}$$

Therefore from this upper bound and the lower bound $\ell \geq -n = 0$, the degeneracy factor in the cylindrical coordinate is given by Eq. (4.13).

Higher excited states with $n \geq 1$ are calculated in a similar way to ground states:

$$\begin{aligned}
\psi_{n\ell}(z, \bar{z}) &\propto (a^\dagger)^n (b^\dagger)^{n+\ell} \psi_{00}(z, \bar{z}) \\
&\propto z^\ell e^{-eBz\bar{z}/4} L_n^\ell (eBz\bar{z}/2) \ ,
\end{aligned} \tag{B.18}$$

which is the same as Eq. (A.23) if we use $z = re^{i\theta}$ and $\bar{z} = re^{-i\theta}$. The upper bound of ℓ for exited states cannot directly be found from Eq. (B.18) while the one for the ground state is derived from the wave function (B.15). Nevertheless the upper bound of ℓ for exited states is obviously $N - n$ because the degeneracy factor N is a common quantity for all Landau levels. From this and the lower bound $\ell \geq -n$, we obtain Eq. (4.14).

Appendix C

Nambu–Jona-Lasinio model

In this chapter, we review the basics of the Nambu–Jona-Lasinio (NJL) model, which is the fundamental framework in this thesis. For the clarification of the correspondence between this effective model and the original QCD, we here focus on the two-flavor NJL model. (The following argument is similarly applicable to the one-flavor NJL model, which be utilized in Chapters 3 and 4.)

In the two-flavor NJL model, the corresponding Lagrangian is given by

$$\mathcal{L}_{\text{NJL}} = \bar{\psi}\left(i\gamma^\mu \partial_\mu - M_0\right)\psi + \frac{G}{2}\left[(\bar{\psi}\psi)^2 + (\bar{\psi}i\gamma_5\psi)^2\right] , \tag{C.1}$$

with $\psi = (u, d)^T$. The first part is the Dirac Lagrangian for free fermions with the current mass $M_0 = \text{diag}(m_u, m_d)$. The second denotes the four-fermi interaction vortex. Here G is the dimensionful coupling constant, which is one of the parameters of the NJL model. For $m_u = m_d = 0$, the above Lagrangian is invariant under the transformation

$$\psi \to e^{i\theta_{\text{V}}}\psi , \quad \psi \to e^{i\gamma_5\theta_{\text{A}}}\psi . \tag{C.2}$$

Hence chiral symmetry $SU_{\text{L}}(2) \times SU_{\text{R}}(2)$ is unbroken in the classical (tree) level of Eq. (C.1), as well as the original Lagrangian of QCD (1.1). However the NJL model realizes the dynamical breaking of chiral symmetry, and the following order parameter becomes finite:

$$\langle \bar{q}q \rangle = -\frac{1}{\beta V}\frac{\partial \ln Z_{\text{NJL}}}{\partial m_q} \quad (\text{ for } q = u, d) , \tag{C.3}$$

which is called chiral condensate.

To see this, we analyze the thermodynamics of the NJL model. Employing the imaginary time formalism, the partition function reads

$$Z_{\text{NJL}} = \int \mathcal{D}\bar{\psi}\mathcal{D}\psi \exp\left[-\int_0^\beta d\tau \int d^3x \, \mathcal{L}_{\text{NJL}}(\psi, \bar{\psi})\right] . \tag{C.4}$$

The functional integration for fermion fields is calculated with the Hubbard–Stranovich transformation; the integration with respect to ψ and $\bar{\psi}$ are replaced with that of the auxiliary field

$\Sigma = \sigma + i\gamma_5\boldsymbol{\tau} \cdot \boldsymbol{\pi}$. For the degenerate two-flavor case with $m_u = m_d = m_0$, we obtain the following expression:

$$Z_{\mathrm{NJL}} = \int \mathcal{D}\Sigma\, e^{-\beta V \Gamma_{\mathrm{eff}}[\Sigma]},$$

$$\Gamma_{\mathrm{eff}}[\Sigma] = \frac{G}{2\beta V} \int_0^\beta d\tau \int d^3x\, |\Sigma(x)|^2 - \frac{N_{\mathrm{f}} N_{\mathrm{c}}}{\beta V} \mathrm{Tr}\ln\left[-i\gamma_4\partial_\tau - i\boldsymbol{\gamma} \cdot \boldsymbol{\nabla} + m_0 + G\Sigma(x)\right], \tag{C.5}$$

where we define $\gamma^0 = -i\gamma_4$, and Tr represents the traces in terms of the spinor and momentum phase space. We now calculate the effective action in the mean-field approximation. Namely, we assume that the dominant contribution of the Σ-integration comes from the stationary point that is the solution for $\delta\Gamma_{\mathrm{eff}}/\delta\Sigma(x) = 0$. Besides let us take the homogeneous real solution: $\Sigma(x) = \Sigma^\dagger(x) = \bar{\sigma}$. In this case, the logarithmic term is calculated in the same manner as that for free fermions. As a result, the effective potential is reduced to

$$\Gamma_{\mathrm{eff}}(m) = \frac{(m-m_0)^2}{2G} - 4N_{\mathrm{f}} N_{\mathrm{c}} \int \frac{d^3p}{(2\pi)^3}\left[\frac{\sqrt{p^2+m^2}}{2} + T\ln\left(1 + e^{-\beta\sqrt{p^2+m^2}}\right)\right] \tag{C.6}$$

with $m = m_0 + G\bar{\sigma}$. We note that the factor $4N_{\mathrm{f}} N_{\mathrm{c}}$ corresponds to the internal degrees of freedom for quarks: fermion/antifermion, spin-up/spin-down, flavor ($N_{\mathrm{f}} = 2$), and color ($N_{\mathrm{c}} = 3$). As is well-known, the first and second term in the integrand are the vacuum and the thermal contribution, respectively. From Eq. (C.6), we confirm that the constituent quark mass is generated through the chiral symmetry breaking, as follows:

$$\langle\bar{\psi}\psi\rangle = -\frac{1}{\beta V}\frac{\partial \ln Z_{\mathrm{NJL}}}{\partial m_0} = \frac{\partial \Gamma_{\mathrm{eff}}}{\partial m_0} = -\frac{m-m_0}{G}. \tag{C.7}$$

As well as the stationary point $\bar{\sigma}$, the dynamical mass m is determined from

$$\frac{\partial \Gamma_{\mathrm{eff}}(m)}{\partial m} = 0, \tag{C.8}$$

which is so-called the gap equation. In the present case, this equation is equivalent to the condition that the dynamical mass m gives a local minimum of the effective thermodynamic potential Γ_{eff}. The gap equation is analytically reduced to

$$\frac{m-m_0}{G} = 4N_{\mathrm{f}} N_{\mathrm{c}} m \int \frac{d^3p}{(2\pi)^3}\frac{1}{\sqrt{p^2+m^2}}\left[\frac{1}{2} - \frac{1}{e^{\beta\sqrt{p^2+m^2}}+1}\right], \tag{C.9}$$

and especially for $m_0 = T = 0$, the equation to determine the nonzero dynamical mass is written as

$$\frac{1}{G} = 2N_{\mathrm{f}} N_{\mathrm{c}} \int \frac{d^3p}{(2\pi)^3}\frac{1}{\sqrt{p^2+m^2}}. \tag{C.10}$$

Once the momentum integral is regularized with a cutoff scheme (see the following discussion in IV), the right hand side is a monotonically decreasing function of m. Therefore there exists a nontrivial solution only if G is larger than the following critical value:

$$G_c = \left[2N_{\mathrm{f}} N_{\mathrm{c}} \int \frac{d^3p}{(2\pi)^3}\frac{1}{p}\right]^{-1}. \tag{C.11}$$

If the nontrivial solution $m \neq 0$ satisfies $\Gamma_{\text{eff}}(m) < \Gamma_{\text{eff}}(0)$, it is the dynamical mass that we seek, and then we find that the chiral broken phase is the ground state. In fact, a nonzero solution for Eq. (C.10) is always the global minimum of $\Gamma_{\text{eff}}(m)$, which implies to the second order chiral phase transition. In finite-density systems, it is known that the phase transition becomes first order. We here mention several remarks about the above argument.

(I) Vafa–Witten theorem

For the stationary condition $\delta\Gamma_{\text{eff}}/\delta\Sigma = 0$, we consider only the scalar condensate; $\sigma = \bar{\sigma}$ and $\boldsymbol{\pi} = \mathbf{0}$. Within the framework of the NJL model, there is no restriction for the emergence of the pseudoscalar condensate. Indeed the scalar and pseudoscalar solutions interchanges each other through an axial rotation. However the pseudoscalar condensation cannot take place because of the Vafa-Witten theorem [123]; vector-like symmetries cannot be spontaneously broken in a vector-like theory (e.g. QCD). We note that the positivity of the Dirac determinant is required for the Vafa-Witten theorem. For this reason, this theorem is not applicable to the system with chemical potential, θ-angle, or electric field, where the lattice QCD simulation suffers from the sign problem. Also for rotation, the pseudoscalar condensate can generally becomes nonzero because the rotational energy shift plays the role of an effective chemical potential. In this thesis we investigate only the scalar condensate in rotating systems, and we leave the analysis of the pseudoscalar condensation induced by rotation as a future work.

(II) Axial anomaly

Since the baryon number should also be conserved due to the Vafa-Witten theorem, the original flavor symmetry in QCD is broken down as follows:

$$U_{\text{L}}(N_{\text{f}}) \times U_{\text{R}}(N_{\text{f}}) \simeq SU_{\text{L}}(N_{\text{f}}) \times SU_{\text{R}}(N_{\text{f}}) \times U_{\text{V}}(1) \times U_{\text{A}}(1) \longrightarrow SU_{\text{V}}(N_{\text{f}}) \times U_{\text{V}}(1). \quad \text{(C.12)}$$

Here $U_{\text{A}}(1)$ is explicitly (not dynamically) broken through a quantum anomaly. In the present NJL model, we do not consider the breaking of the $U_{\text{A}}(1)$ symmetry. For this point, the NJL model is modified with introducing the following new term:

$$\mathcal{L}_{\text{KMT}} = K \left[\det \bar{\psi}(1 + \gamma_5)\psi + \det \bar{\psi}(1 + \gamma_5)\psi \right], \quad \text{(C.13)}$$

which is called the Kobayashi–Masukawa–'t Hooft (KMT) term [124, 125]. In the NJL model, this new term explains the origin of the large mass of η'. Since the main purpose in this thesis is to clarify the dynamical breaking of chiral symmetry, the KMT vortex is not taken into account in Chapters 3 and 4.

(III) Large N_{c} limit and mean-field approximation

Here let us consider the large N_{c} limit. In the model Lagrangian (C.1), the coupling G should be $O(1/N_{\text{c}})$ so that the interaction term is $O(N_{\text{c}})$, as well as the kinetic part. This

means that the 1-loop contribution dominates Z_{NJL} in the large N_{c} limit. Therefore the above analysis under the mean-field approximation is equivalent to the one in the large N_{c} limit. In Chapters 3 and 4, we also consider only such a leading order contribution.

(IV) Cutoff scheme

Since the mass-dimension of the four-fermi interaction part is six, the NJL model is unrenormalizable. Indeed in Eq. (C.9), the momentum integration of the vacuum contribution includes diverges in the ultraviolet region. This implies that the dynamical mass depends on the choice of the momentum cutoff scheme. First let us adopt the three-dimensional cutoff scheme with Λ. Namely, we rewrite the gap equation (C.10) into

$$\frac{1}{G} = 2N_{\mathrm{f}}N_{\mathrm{c}}\frac{4\pi}{(2\pi)^3}\int_0^\Lambda \frac{dp\, p^2}{\sqrt{p^2+m^2}}\,, \tag{C.14}$$

where the momentum integral can be performed analytically at zero temperature. The dynamical mass is obtained by solving the above equation self-consistently. Practically, to analyze the chiral symmetry breaking based on Eq. (C.1), the model parameters G and Λ are adopted so that they reproduce physical quantities. For example, when the pion mass $m_\pi = 138\,\mathrm{MeV}$ and the pion decay constant $f_\pi = 93\,\mathrm{MeV}$ are chosen as the fixed physical quantities, we obtain $\Lambda = 631\,\mathrm{MeV}$ and $G/2 = 0.214\,\mathrm{fm}^2$ for $(m_u + m_d)/2 = 5.5\,\mathrm{MeV}$ [10].

From the viewpoint of the numerical calculation, such a simple cutoff can lead to an undesirable artifact if the momentum integration is substituted with the discrete sum. This is the case with rotation or magnetic field, as we discuss in Chapters 3 and 4. For this reason, in this thesis, we employ the following function:

$$f(p\,;\Lambda,\delta\Lambda) = \frac{\sinh(\Lambda/\delta\Lambda)}{\cosh(p/\delta\Lambda) + \cosh(\Lambda/\delta\Lambda)}\,, \tag{C.15}$$

where p is the modulus of the momentum. The parameter $\delta\Lambda$ represents the smoothness of the cutoff function $f(p\,;\Lambda,\delta\Lambda)$. In the limit of $\delta\Lambda \to 0$, for example, $f(p\,;\Lambda,\delta\Lambda)$ becomes the shape cutoff function, i.e. $\theta(\Lambda^2 - p^2)$. To avoid severe artifacts, the smoothness of $f(p\,;\Lambda,\delta\Lambda)$ is much important in our calculation.

References

[1] D. J. Gross and F. Wilczek, "Ultraviolet Behavior of Nonabelian Gauge Theories," *Phys. Rev. Lett.* **30** (1973) 1343–1346.

[2] H. D. Politzer, "Reliable Perturbative Results for Strong Interactions?," *Phys. Rev. Lett.* **30** (1973) 1346–1349.

[3] **CTEQ** Collaboration, R. Brock *et al.*, "Handbook of perturbative QCD: Version 1.0," *Rev. Mod. Phys.* **67** (1995) 157–248.

[4] Y. Nambu, "Quasiparticles and Gauge Invariance in the Theory of Superconductivity," *Phys. Rev.* **117** (1960) 648–663.

[5] J. Goldstone, "Field Theories with Superconductor Solutions," *Nuovo Cim.* **19** (1961) 154–164.

[6] J. Goldstone, A. Salam, and S. Weinberg, "Broken Symmetries," *Phys. Rev.* **127** (1962) 965–970.

[7] Y. Nambu and G. Jona-Lasinio, "Dynamical Model of Elementary Particles Based on an Analogy with Superconductivity. I," *Phys. Rev.* **122** (1961) 345–358.

[8] Y. Nambu and G. Jona-Lasinio, "Dynamical Model of Elementary Particles Based on an Analogy with Superconductivity. II," *Phys. Rev.* **124** (1961) 246–254.

[9] J. Bardeen, L. N. Cooper, and J. R. Schrieffer, "Theory of superconductivity," *Phys. Rev.* **108** (1957) 1175–1204.

[10] T. Hatsuda and T. Kunihiro, "QCD phenomenology based on a chiral effective Lagrangian," *Phys. Rept.* **247** (1994) 221–367, `arXiv:hep-ph/9401310 [hep-ph]`.

[11] U. Vogl and W. Weise, "The Nambu and Jona Lasinio model: Its implications for hadrons and nuclei," *Prog. Part. Nucl. Phys.* **27** (1991) 195–272.

[12] K. Kashiwa, H. Kouno, T. Sakaguchi, M. Matsuzaki, and M. Yahiro, "Chiral phase transition in an extended NJL model with higher-order multi-quark interactions," *Phys. Lett.* **B647** (2007) 446–451, `arXiv:nucl-th/0608078 [nucl-th]`.

[13] R. D. Pisarski and F. Wilczek, "Remarks on the Chiral Phase Transition in Chromodynamics," *Phys. Rev.* **D29** (1984) 338–341.

[14] F. Wilczek, "Application of the renormalization group to a second order QCD phase transition," *Int. J. Mod. Phys.* **A7** (1992) 3911–3925. [Erratum: Int. J. Mod. Phys.A7,6951(1992)].

[15] F. R. Brown, F. P. Butler, H. Chen, N. H. Christ, Z.-h. Dong, W. Schaffer, L. I. Unger, and A. Vaccarino, "On the existence of a phase transition for QCD with three light quarks," *Phys. Rev. Lett.* **65** (1990) 2491–2494.

[16] C. DeTar and U. M. Heller, "QCD Thermodynamics from the Lattice," *Eur. Phys. J.* **A41** (2009) 405–437, arXiv:0905.2949 [hep-lat].

[17] M. Asakawa and K. Yazaki, "Chiral Restoration at Finite Density and Temperature," *Nucl. Phys.* **A504** (1989) 668–684.

[18] M. A. Stephanov, "QCD phase diagram and the critical point," *Prog. Theor. Phys. Suppl.* **153** (2004) 139–156, arXiv:hep-ph/0402115 [hep-ph]. [Int. J. Mod. Phys.A20,4387(2005)].

[19] M. A. Stephanov, K. Rajagopal, and E. V. Shuryak, "Event-by-event fluctuations in heavy ion collisions and the QCD critical point," *Phys. Rev.* **D60** (1999) 114028, arXiv:hep-ph/9903292 [hep-ph].

[20] **STAR** Collaboration, M. M. Aggarwal *et al.*, "An Experimental Exploration of the QCD Phase Diagram: The Search for the Critical Point and the Onset of De-confinement," arXiv:1007.2613 [nucl-ex].

[21] B.-l. Cheng and A. V. Olinto, "Primordial magnetic fields generated in the quark - hadron transition," *Phys. Rev.* **D50** (1994) 2421–2424.

[22] G. Baym, D. Bodeker, and L. D. McLerran, "Magnetic fields produced by phase transition bubbles in the electroweak phase transition," *Phys. Rev.* **D53** (1996) 662–667, arXiv:hep-ph/9507429 [hep-ph].

[23] D. Grasso and H. R. Rubinstein, "Magnetic fields in the early universe," *Phys. Rept.* **348** (2001) 163–266, arXiv:astro-ph/0009061 [astro-ph].

[24] R. C. Duncan and C. Thompson, "Formation of very strongly magnetized neutron stars - implications for gamma-ray bursts," *Astrophys. J.* **392** (1992) L9.

[25] V. Skokov, A. Yu. Illarionov, and V. Toneev, "Estimate of the magnetic field strength in heavy-ion collisions," *Int. J. Mod. Phys.* **A24** (2009) 5925–5932, arXiv:0907.1396 [nucl-th].

[26] V. Voronyuk, V. D. Toneev, W. Cassing, E. L. Bratkovskaya, V. P. Konchakovski, and S. A. Voloshin, "(Electro-)Magnetic field evolution in relativistic heavy-ion collisions," *Phys. Rev.* **C83** (2011) 054911, `arXiv:1103.4239 [nucl-th]`.

[27] W.-T. Deng and X.-G. Huang, "Event-by-event generation of electromagnetic fields in heavy-ion collisions," *Phys. Rev.* **C85** (2012) 044907, `arXiv:1201.5108 [nucl-th]`.

[28] K. G. Klimenko, "Three-dimensional Gross-Neveu model at nonzero temperature and in an external magnetic field," *Z. Phys.* **C54** (1992) 323–330.

[29] V. P. Gusynin, V. A. Miransky, and I. A. Shovkovy, "Catalysis of dynamical flavor symmetry breaking by a magnetic field in (2+1)-dimensions," *Phys. Rev. Lett.* **73** (1994) 3499–3502, `arXiv:hep-ph/9405262 [hep-ph]`. [Erratum: Phys. Rev. Lett.76,1005(1996)].

[30] V. P. Gusynin, V. A. Miransky, and I. A. Shovkovy, "Dimensional reduction and catalysis of dynamical symmetry breaking by a magnetic field," *Nucl. Phys.* **B462** (1996) 249–290, `arXiv:hep-ph/9509320 [hep-ph]`.

[31] D. Ebert, K. G. Klimenko, M. A. Vdovichenko, and A. S. Vshivtsev, "Magnetic oscillations in dense cold quark matter with four fermion interactions," *Phys. Rev.* **D61** (1999) 025005, `arXiv:hep-ph/9905253 [hep-ph]`.

[32] E. S. Fraga and A. J. Mizher, "Chiral transition in a strong magnetic background," *Phys. Rev.* **D78** (2008) 025016, `arXiv:0804.1452 [hep-ph]`.

[33] E. S. Fraga and L. F. Palhares, "Deconfinement in the presence of a strong magnetic background: an exercise within the MIT bag model," *Phys. Rev.* **D86** (2012) 016008, `arXiv:1201.5881 [hep-ph]`.

[34] G. S. Bali, F. Bruckmann, G. Endrodi, Z. Fodor, S. D. Katz, and A. Schafer, "QCD quark condensate in external magnetic fields," *Phys. Rev.* **D86** (2012) 071502, `arXiv:1206.4205 [hep-lat]`.

[35] C. V. Johnson and A. Kundu, "External Fields and Chiral Symmetry Breaking in the Sakai-Sugimoto Model," *JHEP* **12** (2008) 053, `arXiv:0803.0038 [hep-th]`.

[36] I. A. Shovkovy, "Magnetic Catalysis: A Review," *Lect. Notes Phys.* **871** (2013) 13–49, `arXiv:1207.5081 [hep-ph]`.

[37] V. A. Miransky and I. A. Shovkovy, "Quantum field theory in a magnetic field: From quantum chromodynamics to graphene and Dirac semimetals," *Phys. Rept.* **576** (2015) 1–209, `arXiv:1503.00732 [hep-ph]`.

[38] E. V. Gorbar, V. P. Gusynin, and V. A. Miransky, "Toward theory of quantum Hall effect in graphene," *Low Temp. Phys.* **34** (2008) 790, `arXiv:0710.3527 [cond-mat.mes-hall]`.

[39] E. V. Gorbar, V. P. Gusynin, V. A. Miransky, and I. A. Shovkovy, "Dynamics in the quantum Hall effect and the phase diagram of graphene," *Phys. Rev.* **B78** (2008) 085437, `arXiv:0806.0846 [cond-mat.mes-hall]`.

[40] B. Roy and J. D. Sau, "Magnetic Catalysis and Spontaneous Mass Generation in Weyl Semimetals," *Phys. Rev.* **B92** no. 12, (2015) 125141, `arXiv:1406.4501 [cond-mat.mes-hall]`.

[41] F. Preis, A. Rebhan, and A. Schmitt, "Inverse magnetic catalysis in dense holographic matter," *JHEP* **03** (2011) 033, `arXiv:1012.4785 [hep-th]`.

[42] F. Preis, A. Rebhan, and A. Schmitt, "Inverse magnetic catalysis in field theory and gauge-gravity duality," *Lect. Notes Phys.* **871** (2013) 51–86, `arXiv:1208.0536 [hep-ph]`.

[43] N. K. Wilkin and J. M. F. Gunn, "Condensation of 'Composite Bosons' in a Rotating BEC," *Phys. Rev. Lett.* **84** (2000) 6–9.

[44] N. R. Cooper, N. K. Wilkin, and J. M. F. Gunn, "Quantum Phases of Vortices in Rotating Bose-Einstein Condensates," *Phys. Rev. Lett.* **87** (2001) 120405.

[45] V. Schweikhard, I. Coddington, P. Engels, V. P. Mogendorff, and E. A. Cornell, "Rapidly Rotating Bose-Einstein Condensates in and near the Lowest Landau Level," *Phys. Rev. Lett.* **92** (2004) 040404, `arXiv:cond-mat/0308582 [cond-mat.mes-hall]`.

[46] S. Viefers, "Quantum hall physics in rotating bose–einstein condensates," *J. of Phys.: Cond. Matt.* **20** no. 12, (2008) 123202.

[47] A. L. Fetter, "Rotating trapped Bose-Einstein condensates," *Rev. Mod. Phys.* **81** (2009) 647–691.

[48] M. Tsubota, K. Kasamatsu, and M. Kobayashi, "Quantized vortices in superfluid helium and atomic bose-einstein condensates," `arXiv:1004.5458 [cond-mat.quant-gas]`.

[49] Z.-T. Liang and X.-N. Wang, "Globally polarized quark-gluon plasma in non-central A+A collisions," *Phys. Rev. Lett.* **94** (2005) 102301, `arXiv:nucl-th/0410079 [nucl-th]`. [Erratum: Phys. Rev. Lett.96,039901(2006)].

[50] X.-G. Huang, P. Huovinen, and X.-N. Wang, "Quark Polarization in a Viscous Quark-Gluon Plasma," *Phys. Rev.* **C84** (2011) 054910, `arXiv:1108.5649 [nucl-th]`.

[51] X.-G. Huang, "Electromagnetic fields and anomalous transports in heavy-ion collisions — A pedagogical review," *Rept. Prog. Phys.* **79** no. 7, (2016) 076302, arXiv:1509.04073 [nucl-th].

[52] Y. Jiang, Z.-W. Lin, and J. Liao, "Rotating quark-gluon plasma in relativistic heavy ion collisions," arXiv:1602.06580 [hep-ph].

[53] A. Aristova, D. Frenklakh, A. Gorsky, and D. Kharzeev, "Vortical susceptibility of finite-density QCD matter," arXiv:1606.05882 [hep-ph].

[54] W.-T. Deng and X.-G. Huang, "Vorticity in Heavy-Ion Collisions," *Phys. Rev.* **C93** no. 6, (2016) 064907, arXiv:1603.06117 [nucl-th].

[55] D. E. Kharzeev, L. D. McLerran, and H. J. Warringa, "The Effects of topological charge change in heavy ion collisions: 'Event by event P and CP violation'," *Nucl. Phys.* **A803** (2008) 227–253, arXiv:0711.0950 [hep-ph].

[56] K. Fukushima, D. E. Kharzeev, and H. J. Warringa, "The Chiral Magnetic Effect," *Phys. Rev.* **D78** (2008) 074033, arXiv:0808.3382 [hep-ph].

[57] D. Kharzeev and A. Zhitnitsky, "Charge separation induced by P-odd bubbles in QCD matter," *Nucl. Phys.* **A797** (2007) 67–79, arXiv:0706.1026 [hep-ph].

[58] D. T. Son and P. Surowka, "Hydrodynamics with Triangle Anomalies," *Phys. Rev. Lett.* **103** (2009) 191601, arXiv:0906.5044 [hep-th].

[59] D. E. Kharzeev, J. Liao, S. A. Voloshin, and G. Wang, "Chiral Magnetic Effect in High-Energy Nuclear Collisions — A Status Report," arXiv:1511.04050 [hep-ph].

[60] K. Mameda and A. Yamamoto, "Magnetism and rotation in relativistic field theory," *Prog. Theor. Exp. Phys.* **2016** (2016) 093B05, arXiv:1504.05826 [hep-th].

[61] L. Parker and D. Toms, *Quantum field theory in curved spacetime: quantized fields and gravity.* Cambridge University Press, 2009.

[62] E. Elizalde, S. Leseduarte, and S. D. Odintsov, "Chiral symmetry breaking in the Nambu-Jona-Lasinio model in curved space-time with nontrivial topology," *Phys. Rev.* **D49** (1994) 5551–5558, arXiv:hep-th/9312164 [hep-th].

[63] T. Inagaki, T. Muta, and S. D. Odintsov, "Nambu-Jona-Lasinio model in curved space-time," *Mod. Phys. Lett.* **A08** (1993) 2117–2124, arXiv:hep-th/9306023 [hep-th].

[64] T. Inagaki, T. Muta, and S. D. Odintsov, "Dynamical symmetry breaking in curved space-time: Four fermion interactions," *Prog. Theor. Phys. Suppl.* **127** (1997) 93, `arXiv:hep-th/9711084 [hep-th]`.

[65] E. V. Gorbar, "Dynamical symmetry breaking in spaces with constant negative curvature," *Phys. Rev.* **D61** (1999) 024013, `arXiv:hep-th/9904180 [hep-th]`.

[66] X.-G. Huang, X.-W. Hao, and P.-F. Zhuang, "Chiral phase structure at finite temperature and density in Einstein universe," *Astropart. Phys.* **28** (2007) 472–480, `arXiv:hep-ph/0602186 [hep-ph]`.

[67] R. Schutzhold, "Small cosmological constant from the QCD trace anomaly?," *Phys. Rev. Lett.* **89** (2002) 081302, `arXiv:gr-qc/0204018 [gr-qc]`.

[68] F. R. Urban and A. R. Zhitnitsky, "The QCD nature of Dark Energy," *Nucl. Phys.* **B835** (2010) 135–173, `arXiv:0909.2684 [astro-ph.CO]`.

[69] A. Flachi and T. Tanaka, "Chiral Phase Transitions around Black Holes," *Phys. Rev.* **D84** (2011) 061503, `arXiv:1106.3991 [hep-th]`.

[70] A. Flachi, "Deconfinement transition and Black Holes," *Phys. Rev.* **D88** no. 4, (2013) 041501, `arXiv:1305.5348 [hep-th]`.

[71] A. Flachi and K. Fukushima, "Chiral Mass-Gap in Curved Space," *Phys. Rev. Lett.* **113** no. 9, (2014) 091102, `arXiv:1406.6548 [hep-th]`.

[72] S. Benic and K. Fukushima, "Unruh effect and condensate in and out of an accelerated vacuum," `arXiv:1503.05790 [hep-th]`.

[73] A. Yamamoto and Y. Hirono, "Lattice QCD in rotating frames," *Phys. Rev. Lett.* **111** (2013) 081601, `arXiv:1303.6292 [hep-lat]`.

[74] A. Yamamoto, "Lattice QCD in curved spacetimes," *Phys. Rev.* **D90** no. 5, (2014) 054510, `arXiv:1405.6665 [hep-lat]`.

[75] S. Benic and A. Yamamoto, "Quantum Monte Carlo simulation with a black hole," `arXiv:1603.00716 [hep-lat]`.

[76] H.-L. Chen, K. Fukushima, X.-G. Huang, and K. Mameda, "Analogy between rotation and density for Dirac fermions in a magnetic field," *Phys. Rev.* **D93** no. 10, (2016) 104052, `arXiv:1512.08974 [hep-ph]`.

[77] Y. Jiang and J. Liao, "Pairing Phase Transitions of Matter under Rotation," *Phys. Rev. Lett.* **117** no. 19, (2016) 192302, `arXiv:1606.03808 [hep-ph]`.

[78] K. Hattori and Y. Yin, "Charge redistribution from anomalous magnetovorticity coupling," *Phys. Rev. Lett.* **117** no. 15, (2016) 152002, `arXiv:1607.01513 [hep-th]`.

[79] M. N. Chernodub and S. Gongyo, "Interacting fermions in rotation: chiral symmetry restoration, moment of inertia and thermodynamics," `arXiv:1611.02598 [hep-th]`.

[80] S. Ebihara, K. Fukushima, and K. Mameda, "Boundary effects and gapped dispersion in rotating fermionic matter," *Phys. Lett.* **B764** (2017) 94–99, `arXiv:1608.00336 [hep-ph]`.

[81] A. Vilenkin, "Parity Violating Currents in Thermal Radiation," *Phys. Lett.* **B80** (1978) 150–152.

[82] A. Vilenkin, "Macroscopic parity violating effects: Neutrino fluxes from rotating black holes and in rotating thermal radiation," *Phys. Rev.* **D20** (1979) 1807–1812.

[83] A. Vilenkin, "Quantum field theory at finite temperature in a rotating system," *Phys. Rev.* **D21** (1980) 2260–2269.

[84] L. D. Landau and E. M. Lifshitz, "Statistical physics," *Course of Theoretical Physics* **5** (1958) .

[85] B. R. Iyer, "Dirac field theory in rotating coordinates," *Phys. Rev.* **D26** (1982) 1900–1905.

[86] F. W. Hehl and W.-T. Ni, "Inertial effects of a Dirac particle," *Phys. Rev.* **D42** (1990) 2045–2048.

[87] C. Giordano and A. Laforgia, "Elementary approximations for zeros of bessel functions," *Journal of Computational and Applied Mathematics* **9** no. 3, (1983) 221 – 228.

[88] V. E. Ambrus and E. Winstanley, "Rotating fermions inside a cylindrical boundary," *Phys. Rev.* **D93** no. 10, (2016) 104014, `arXiv:1512.05239 [hep-th]`.

[89] M. Hortacsu, K. D. Rothe, and B. Schroer, "Zero Energy Eigenstates for the Dirac Boundary Problem," *Nucl. Phys.* **B171** (1980) 530–542.

[90] M. Buballa and S. Carignano, "Inhomogeneous chiral condensates," *Prog. Part. Nucl. Phys.* **81** (2015) 39–96, `arXiv:1406.1367 [hep-ph]`.

[91] T. D. . Cohen, "Functional integrals for QCD at nonzero chemical potential and zero density," *Phys. Rev. Lett.* **91** (2003) 222001, `arXiv:hep-ph/0307089 [hep-ph]`.

[92] N. Banerjee, J. Bhattacharya, S. Bhattacharyya, S. Dutta, R. Loganayagam, and P. Surowka, "Hydrodynamics from charged black branes," *JHEP* **01** (2011) 094, `arXiv:0809.2596 [hep-th]`.

[93] J. Erdmenger, M. Haack, M. Kaminski, and A. Yarom, "Fluid dynamics of R-charged black holes," *JHEP* **01** (2009) 055, `arXiv:0809.2488 [hep-th]`.

[94] A. Flachi and K. Fukushima, "Chiral vortical effect in curved space and the Chern-Simons current," `arXiv:1702.04753 [hep-th]`.

[95] F. W. J. Olver, "On Bessel functions of large order," *Phil. Trans. Roy. Soc. Lond.* **A247** (1954) 328–368.

[96] D. T. Son and A. R. Zhitnitsky, "Quantum anomalies in dense matter," *Phys. Rev.* **D70** (2004) 074018, `arXiv:hep-ph/0405216 [hep-ph]`.

[97] M. A. Metlitski and A. R. Zhitnitsky, "Anomalous axion interactions and topological currents in dense matter," *Phys. Rev.* **D72** (2005) 045011, `arXiv:hep-ph/0505072 [hep-ph]`.

[98] D. E. Kharzeev and H.-U. Yee, "Chiral Magnetic Wave," *Phys. Rev.* **D83** (2011) 085007, `arXiv:1012.6026 [hep-th]`.

[99] N. Brambilla *et al.*, "QCD and Strongly Coupled Gauge Theories: Challenges and Perspectives," *Eur. Phys. J.* **C74** no. 10, (2014) 2981, `arXiv:1404.3723 [hep-ph]`.

[100] K. Fukushima, "Views of the Chiral Magnetic Effect," *Lect. Notes Phys.* **871** (2013) 241–259, `arXiv:1209.5064 [hep-ph]`.

[101] D. E. Kharzeev, "The Chiral Magnetic Effect and Anomaly-Induced Transport," *Prog. Part. Nucl. Phys.* **75** (2014) 133–151, `arXiv:1312.3348 [hep-ph]`.

[102] S. Ebihara, K. Fukushima, and T. Oka, "Chiral pumping effect induced by rotating electric fields," *Phys. Rev.* **B93** no. 15, (2016) 155107, `arXiv:1509.03673 [cond-mat.str-el]`.

[103] W. De Haas and P. van Alphen, "The dependence of the susceptibility of diamagnetic metals upon the field," in *Proc. Netherlands Roy. Acad. Sci*, vol. 33, p. 170. 1930.

[104] W. De Haas and P. Van Alphen, "Oscillations in the magnetization of bismuth," *Leiden Commun* **208** (1930) 212a–212a.

[105] P. C. W. Davies, T. Dray, and C. A. Manogue, "The Rotating quantum vacuum," *Phys. Rev.* **D53** (1996) 4382–4387, `arXiv:gr-qc/9601034 [gr-qc]`.

[106] G. Duffy and A. C. Ottewill, "The Rotating quantum thermal distribution," *Phys. Rev.* **D67** (2003) 044002, `arXiv:hep-th/0211096 [hep-th]`.

[107] J. S. Schwinger, "On gauge invariance and vacuum polarization," *Phys. Rev.* **82** (1951) 664–679.

[108] E. V. Gorbar, V. A. Miransky, and I. A. Shovkovy, "Normal ground state of dense relativistic matter in a magnetic field," *Phys. Rev.* **D83** (2011) 085003, `arXiv:1101.4954 [hep-ph]`.

[109] W. Wang, H. Hofmann, and C. Bakis, "Ultrahigh speed permanent magnet motor/generator for aerospace flywheel energy storage applications," in *IEEE International Conference on Electric Machines and Drives, 2005.*, pp. 1494–1500, IEEE. 2005.

[110] K. S. Novoselov, A. K. Geim, S. V. Morozov, D. Jiang, M. I. Katsnelson, I. V. Grigorieva, S. V. Dubonos, and A. A. Firsov, "Two-dimensional gas of massless Dirac fermions in graphene," *Nature* **438** (2005) 197, `arXiv:cond-mat/0509330 [cond-mat.mes-hall]`.

[111] L. P. Csernai, V. K. Magas, H. Stocker, and D. D. Strottman, "Fluid Dynamical Prediction of Changed v1-flow at LHC," *Phys. Rev.* **C84** (2011) 024914, `arXiv:1101.3451 [nucl-th]`.

[112] G. B. Cook, S. L. Shapiro, and S. A. Teukolsky, "Rapidly rotating neutron stars in general relativity: Realistic equations of state," *Astrophys. J.* **424** (1994) 823.

[113] J. Friedman, J. Ipser, and L. Parker, "Rapidly rotating neutron star models," *The Astrophysical Journal* **304** (1986) 115–139.

[114] N. K. Glendenning, S. Pei, and F. Weber, "Signal of quark deconfinement in the timing structure of pulsar spin-down," *Phys. Rev. Lett.* **79** no. 9, (1997) 1603.

[115] E. Chubarian, H. Grigorian, G. Poghosyan, and D. Blaschke, "Deconfinement transition in rotating compact stars," `arXiv:astro-ph/9903489 [astro-ph]`.

[116] P. Haensel, A. Y. Potekhin, and D. G. Yakovlev, *Neutron stars 1: Equation of state and structure*, vol. 326. Springer Science & Business Media, 2007.

[117] P. Kovtun, D. T. Son, and A. O. Starinets, "Viscosity in strongly interacting quantum field theories from black hole physics," *Phys. Rev. Lett.* **94** (2005) 111601, `arXiv:hep-th/0405231 [hep-th]`.

[118] F. Becattini and L. Ferroni, "The Microcanonical ensemble of the ideal relativistic quantum gas with angular momentum conservation," *Eur. Phys. J.* **C52** (2007) 597–615, `arXiv:0707.0793 [nucl-th]`.

[119] F. Becattini and F. Piccinini, "The Ideal relativistic spinning gas: Polarization and spectra," *Annals Phys.* **323** (2008) 2452–2473, `arXiv:0710.5694 [nucl-th]`.

[120] F. Becattini and L. Tinti, "The Ideal relativistic rotating gas as a perfect fluid with spin," *Annals Phys.* **325** (2010) 1566–1594, `arXiv:0911.0864 [gr-qc]`.

[121] F. Becattini, V. Chandra, L. Del Zanna, and E. Grossi, "Relativistic distribution function for particles with spin at local thermodynamical equilibrium," *Annals Phys.* **338** (2013) 32–49, `arXiv:1303.3431 [nucl-th]`.

[122] F. Becattini, G. Inghirami, V. Rolando, A. Del Zanna, L. De Pace, G. Pagliara, and V. Chandra, "A study of vorticity formation in high energy nuclear collisions," *Eur. Phys. J.* **C75** (2015) 406, `arXiv:1501.04468 [nucl-th]`.

[123] C. Vafa and E. Witten, "Parity Conservation in QCD," *Phys. Rev. Lett.* **53** (1984) 535.

[124] M. Kobayashi and T. Maskawa, "Chiral symmetry and eta-x mixing," *Prog. Theor. Phys.* **44** (1970) 1422–1424.

[125] G. 't Hooft, "Computation of the Quantum Effects Due to a Four-Dimensional Pseudoparticle," *Phys. Rev.* **D14** (1976) 3432–3450. [Erratum: Phys. Rev.D18,2199(1978)].